Free Radical Biology and Medicine 208 (2023) 859–876

Contents lists available at ScienceDirect

Free Radical Biology and Medicine

journal homepage: www.elsevier.com/locate/freeradbiomed

Staphylococcus aureus adapts to the immunometabolite itaconic acid by inducing acid and oxidative stress responses including *S*-bacillithiolations and *S*-itaconations

Vu Van Loi [a], Tobias Busche [b], Benno Kuropka [c], Susanne Müller [a], Karen Methling [d], Michael Lalk [d], Jörn Kalinowski [b], Haike Antelmann [a,*]

[a] Freie Universität Berlin, Institute of Biology-Microbiology, D-14195, Berlin, Germany
[b] Microbial Genomics and Biotechnology, Center for Biotechnology, Bielefeld University, D-33615, Bielefeld, Germany
[c] Freie Universität Berlin, Institute of Chemistry and Biochemistry, D-14195, Berlin, Germany
[d] Department of Cellular Biochemistry and Metabolomics, University of Greifswald, 17487, Greifswald, Germany

ARTICLE INFO

Keywords:
Staphylococcus aureus
Itaconic acid
Transcriptome
Metabolome
Itaconation
S-bacillithiolation

ABSTRACT

Staphylococcus aureus is a major pathogen, which has to defend against reactive oxygen and electrophilic species encountered during infections. Activated macrophages produce the immunometabolite itaconate as potent electrophile and antimicrobial upon pathogen infection. In this work, we used transcriptomics, metabolomics and shotgun redox proteomics to investigate the specific stress responses, metabolic changes and redox modifications caused by sublethal concentrations of itaconic acid in *S. aureus*.

In the RNA-seq transcriptome, itaconic acid caused the induction of the GlnR, KdpDE, CidR, SigB, GraRS, PerR, CtsR and HrcA regulons and the urease-encoding operon, revealing an acid and oxidative stress response and impaired proteostasis. Neutralization using external urea as ammonium source improved the growth and decreased the expression of the glutamine synthetase-controlling GlnR regulon, indicating that *S. aureus* experienced ammonium starvation upon itaconic acid stress. In the extracellular metabolome, the amounts of acetate and formate were decreased, while secretion of pyruvate and the neutral product acetoin were strongly enhanced to avoid intracellular acidification. Exposure to itaconic acid affected the amino acid uptake and metabolism as revealed by the strong intracellular accumulation of lysine, threonine, histidine, aspartate, alanine, valine, leucine, isoleucine, cysteine and methionine. In the proteome, itaconic acid caused widespread *S*-bacillithiolation and *S*-itaconation of redox-sensitive antioxidant and metabolic enzymes, ribosomal proteins and translation factors in *S. aureus*, supporting its oxidative and electrophilic mode of action in *S. aureus*. In phenotype analyses, the catalase KatA, the low molecular weight thiol bacillithiol and the urease provided protection against itaconic acid-induced oxidative and acid stress in *S. aureus*. Altogether, our results revealed that under physiological infection conditions, such as in the acidic phagolysosome, itaconic acid is a highly effective antimicrobial against multi-resistant *S. aureus* isolates, which acts as weak acid causing an acid, oxidative and electrophilic stress response, leading to *S*-bacillithiolation and itaconation.

1. Introduction

Staphylococcus aureus is a major human pathogen, which colonizes the skin and the airways of one quarter of the human population without causing symptoms of infections [1]. However, in the hospitals or in immunocompromised persons, *S. aureus* can cause severe and life-threatening diseases, such as sepsis, pneumonia, osteomyelitis or chronic infections [2–4]. Due to the fast genome evolution and spread of multi-resistant *S. aureus* (MRSA) isolates, the treatment options are limited and alternative anti-infective strategies are required, involving the development of novel therapeutics and the discovery of new drug targets [5,6].

During infections and at the sites of colonisations, *S. aureus* has to cope with the respiratory burst of our innate immune system. Activated macrophages and neutrophils produce reactive oxygen and electrophile species (ROS, RES) and (pseudo)hypohalous acids (HOX), such as

* Corresponding author. Institute for Biology-Microbiology, Freie Universität Berlin, Königin-Luise-Strasse 12-16, D-14195, Berlin, Germany.
E-mail address: haike.antelmann@fu-berlin.de (H. Antelmann).

https://doi.org/10.1016/j.freeradbiomed.2023.09.031
Received 14 August 2023; Received in revised form 21 September 2023; Accepted 26 September 2023
Available online 2 October 2023

hypochlorous acid (HOCl), hypobromous acid (HBr) and hypothiocyanous acid (HOSCN), which function as potent antimicrobial weapons to kill the invading pathogens [7–9]. During infections, macrophages activate the Immune-Responsive-Gene 1 (IRG1) to produce the antimicrobial metabolite itaconate, which alters the macrophage metabolism by inhibition of succinate dehydrogenase, aldolase and glyceraldehyde-3-phosphate dehydrogenase [7–11]. *S. aureus* was shown to activate itaconate production by IRG1 via induction of mitochondrial ROS in the airway macrophages [12]. In neutrophils, *S. aureus* stimulates itaconate synthesis, which inhibits glycolysis and the NADPH oxidase leading to impaired pathogen clearance and neutrophil survival [13]. In inflammatory macrophages, itaconate was demonstrated to function as electrophile leading to depletion of the major low molecular weight (LMW) thiol glutathione (GSH) and the activation of the Nuclear factor erythroid-2-related factor 2 (Nfr2) pathway to induce antioxidant functions and electrophile defense mechanisms [14]. Owing to the electrophilic α, β-unsaturated carboxylic acid, itaconate reacts with Cys thiols via the *S*-alkylation chemistry resulting in 2,3-dicarboxypropyl adducts, known as itaconations [15]. Itaconation was reported for important transcriptional regulators and kinases, such as transcription factor EB (TFEB), the Kelch-like ECH-associated protein 1 (KEAP1) as inhibitor of Nrf2, the Janus kinase 1 (JAK1), and the NOD-, LRR- and pyrin domain-containing protein 3 (NLRP3) inflammasome, controlling the antimicrobial and anti-inflammatory activity of macrophages [16–19]. Widespread itaconations were mapped using bioorthogonal probes in the thiol proteome of inflammatory macrophages [20] and in the Gram-negative bacterial pathogen *Salmonella* Typhimurium [21]. The isocitrate lysase (Icl) is the key enzyme of the glyoxylate cycle, which was inactivated by itaconation of Cys195 in *S*. Typhimurium. The Icl-C195S mutant protein caused growth defects in *S.* Typhimurium, indicating that itaconation regulates the assimilation of acetyl-CoA, which is important for gluconeogenesis and survival in many bacterial pathogens [21]. The antimicrobial mode of action of itaconate was studied in *Pseudomonas aeruginosa* and in *S. aureus*, where itaconate inhibited glycolysis and stimulated the biosynthesis of exopolysaccharides (EPS) to induce biofilms associated with chronic infections in the lung [12,22]. These previous studies have been performed by growing the bacteria in pH-controlled itaconate-supplemented LB medium [12,22], which does not consider the strong acidity of itaconic acid (pKa 3.85 and 5.45) [23] as it is naturally produced in macrophages and encountered during infections by *S. aureus* [24]. Thus, the specific stress responses and the redox-active mode of action of itaconic acid under physiological infection-relevant conditions, such as in the acidic phagolysosome of macrophages, remain to be elucidated in *S. aureus*.

To cope with oxidative and electrophile stress, *S. aureus* utilizes several detoxification enzymes and the LMW thiol bacillithiol (BSH), which function in the defense against ROS, HOX, RES and related redox-active antimicrobial compounds to regenerate the cellular redox balance and to promote bacterial survival during infections [25,26]. These defense mechanisms are under the control of redox-sensitive transcription factors, such as PerR, MgrA, SarZ, HypR, QsrR and MhqR, which sense and respond to ROS, HOX or RES via thiol-based switches and other mechanisms, leading to upregulation of detoxification enzymes and providing resistance to multiple thiol-reactive compounds [25–31]. Under oxidative stress, the LMW thiol BSH and its associated bacilliredoxin (Brx)/BSH/bacillithiol disulfide reductase (YpdA) pathways have been shown to function in thiol-protection and redox-regulation of metabolic and antioxidant enzymes and transcriptional regulators via *S*-bacillithiolation and de-bacillithiolation pathways in *S. aureus* [32–34]. The glycolytic glyceraldehyde-3-phosphate dehydrogenase GapA was identified as the major target for *S*-bacillithiolation in *S. aureus* [34,35]. The inactivation of GapA by *S*-bacillithiolation occurred faster compared to the overoxidation-induced inactivation, supporting that *S*-bacillithiolation efficiently protects active site Cys residues to ensure their reactivation during the recovery from oxidative stress [34,35]. However, it is unknown whether itaconic acid causes reversible thiol-oxidations, such as *S*-bacillithiolation or irreversible itaconations via the oxidative or electrophilic modes during infection-relevant conditions in *S. aureus*, respectively.

In this work, we applied RNA-seq transcriptomics, metabolomics and shotgun proteomics to investigate the mode of action of itaconic acid as oxidant and electrophile and to identify its specific stress responses and metabolic changes in *S. aureus*. To study bacterial stress responses under physiological conditions, we used itaconic acid as it is produced inside macrophages without external pH neutralization after stress exposure in line with our previous stress experiments of other antimicrobial acids (e.g. HOCl and HOSCN) [36,37]. Subsequent pH neutralization would affect the bacterial physiology and significantly decrease the antimicrobial activity of itaconic acid [24]. Moreover, *S. aureus* encounters itaconic acid during infections in the acidic phagolysosome of activated macrophages or neutrophils, potentiating the antimicrobial activity of itaconic acid at low pH as shown for *Escherichia coli* and *S.* Typhimurium [24,38,39]. Our results showed that itaconic acid causes mainly an acid stress signature due to its acidification, which is accompanied by oxidative stress, resulting in *S*-bacillithiolation and itaconation of different redox-sensitive antioxidant and metabolic enzymes in the proteome of *S. aureus*. We further detected changes in the uptake of several amino acids in the intracellular metabolome and higher secretion of acetoin to combat acid stress. Phenotypic analyses supported that BSH, the catalase and the urease function in the protection of *S. aureus* against itaconic acid-induced oxidative, electrophile and acid stress. Thus, our study revealed that both acid stress and ROS resistance mechanisms are employed by *S. aureus* to survive the metabolic stress caused by itaconic acid during infections of immune cells.

2. Materials and methods

Bacterial strains, growth and survival assays. The bacterial strains, plasmids and primers for cloning, which are used in this work are described in Tables S1 and S2. For genetic manipulation and cloning, *E. coli* strains containing the pMAD and pRB473 plasmids were grown in Luria Bertani (LB) medium. For stress experiments, we used *S. aureus* COL wild type (WT), Δ*katA*, Δ*bshA*, Δ*ccpA* and Δ*ureABCE* deletion mutants and the *katA, bshA* and *ccpA* complemented strains (Table S1), which were cultivated in RPMI supplemented with 0.75 μM $FeCl_2$ and 2 mM glutamine [40]. The *S. aureus* strains were treated with sub-lethal doses of 13 mM itaconic acid or 13 mM succinic acid during the exponential growth at an OD_{500} of 0.5 as described for other stress experiments [36]. Survival assays were performed by plating 100 μl of serial dilutions of *S. aureus* strains after treatment with lethal doses of 20 mM itaconic acid onto LB agar plates for counting of colony forming units (CFUs). Statistical analysis was performed using Student's unpaired two-tailed *t*-test by the graph prism software. Itaconic acid, succinic acid, sodium hypochlorite, dithiothreitol (DTT) and N-ethyl maleimide (NEM) were purchased from Sigma Aldrich.

RNA isolation, library preparation and next generation cDNA sequencing. *S. aureus* COL was cultivated in RPMI medium until an OD_{500} of 0.5 and harvested before (control) and at 30 min after exposure to 13 mM itaconic acid as described [41]. Three biological replicates of itaconic acid stress experiments were conducted for the RNA-seq transcriptome analysis. Cells were disrupted in 3 mM EDTA/200 mM NaCl lysis buffer with a Precellys24 ribolyzer followed by RNA isolation using the acid phenol extraction protocol as described [42]. The RNA quality was analyzed by Trinean Xpose (Gentbrugge, Belgium) and the Agilent RNA Nano 6000 kit using an Agilent 2100 Bioanalyzer (Agilent Technologies, Böblingen, Germany). Ribo-Zero rRNA Removal Kit (Bacteria) from Illumina (San Diego, CA, USA) was used to remove the stabile rRNA. TruSeq Stranded mRNA Library Prep Kit from Illumina (San Diego, CA, USA) was applied to prepare the cDNA libraries. The cDNAs were sequenced paired end on an Illumina HiSeq 1500 (San Diego, CA, USA) using 70 and 75 bp read length and a minimum sequencing depth of 10 million reads per library. The transcriptome sequencing raw data

files are available in the ArrayExpress database (www.ebi.ac.uk/arrayexpress) under accession number E-MTAB-13287.

Bioinformatics data analysis, read mapping, data visualization and analysis of differential gene expression. The paired end cDNA reads were mapped to the *S. aureus* COL genome sequence (accession number NC_002951) using bowtie2 v2.2.7 [43] with default settings for paired-end read mapping. All mapped sequence data were converted from SAM to BAM format with SAMtools v1.3 [44] and imported to the software ReadXplorer v.2.2 [45].

Differential gene expression analysis of triplicates including normalization was performed using Bioconductor package DESeq2 [46] included in the ReadXplorer v2.2 software [45]. The signal intensity value (A-value) was calculated by log2 mean of normalized read counts and the signal intensity ratio (M-value) by log2 fold-change. The evaluation of the differential RNA-seq data was performed using an adjusted p-value cut-off of $P \leq 0.01$ and a signal intensity ratio (M-value) cut-off of ≥ 1 or ≤ -1. Genes with an M-value outside this range and $p \leq 0.05$ were considered as differentially up- or downregulated under itaconic acid stress. The statistics was calculated by DESeq2 using the Wald test to identify genes that are differentially expressed between two sample classes.

Construction of the *S. aureus* COL Δ*ccpA* and Δ*ureABCE* deletion mutants and complemented strains. The *S. aureus* Δ*ccpA* and Δ*ureABCE* deletion mutants were constructed using the temperature-sensitive shuttle vector pMAD as described previously [36]. For construction of the Δ*ccpA* mutant, 500 bp of the up- and downstream flanking regions of the *ccpA* gene (*SACOL1786*) were amplified by PCR. For the Δ*ureABCE* mutant, the upstream region of the *ureA (SACOL2280)* gene and the downstream region of the *ureE (SACOL2283)* gene were amplified by PCR. The corresponding up- and downstream PCR products were fused by a second overlap extension PCR, digested with *Bgl*II and *Sal*I and ligated into pMAD. The resulting pMAD constructs were electroporated into the restriction-negative intermediate strain *S. aureus* RN4220 for its methylation, followed by phage transduction using phage 81 into *S. aureus* COL. The Δ*ccpA* and Δ*ureABCE* deletion mutants were selected as previously described [36].

For construction of the *ccpA* complemented strain, the *ccpA* gene with its ribosome binding site was amplified by PCR using the primers pRB-ccpA-for-BamHI and pRB-ccpAHis-rev-KpnI from chromosomal DNA of *S. aureus* COL as template (Table S2). The *ccpA* gene was cloned into the *Bam*HI and *Kpn*I restriction sites of the plasmid pRB473. The resulting plasmid pRB473-*ccpA* was electroporated into *S. aureus* RN4220, followed by phage transduction into the *S. aureus* COL Δ*ccpA* mutant strain as described [36].

Northern blot experiments. Northern blot analysis was performed as described previously [47] using RNA isolated from *S. aureus* COL after exposure to 13 mM itaconic acid for 30 and 60 min. Hybridizations were performed using the digoxigenin-labelled antisense RNA probes specific for the genes *glnA* (*SACOL1329*), *ureC (SACOL2282), alsS (SACOL2199),* and *kdpC (SACOL2066*). The probes were synthesized in vitro using T7 RNA polymerase and the gene-specific primers **(**Table S2**)** as described [36,48]. The RNA probes specific for *merA*, *katA* and *ahpC* were previously constructed [36,49]. Quantification of the signals from the Northern blot images was conducted using ImageJ 1.52a. The itaconic acid-induced fold-changes were calculated from 2 to 3 biological replicates and the transcriptional induction of the control was set to 1.

Western blot analysis. *S. aureus* COL WT and the Δ*bshA* mutant were grown in LB until an OD_{540} of 2 and harvested by centrifugation [36]. Cells were transferred to Belitsky minimal medium (BMM) and treated with 13 mM itaconic acid for 30 and 60 min, followed by addition of 50 mM NEM. The cells were harvested by centrifugation, washed in TE-buffer (pH 8.0), disrupted using the ribolyzer and the protein extract was cleared from cell debris by centrifugation. Protein extracts of 25 μg were separated by 15% non-reducing sodium dodecyl sulfate–polyacrylamide gel electrophoresis (SDS–PAGE), followed by BSH-specific Western blot analysis using the polyclonal rabbit anti-BSH antiserum as described previously [33].

Identification of *S*-bacillithiolated and itaconated proteins using Orbitrap Q Exactive Liquid Chromatography-tandem mass spectrometry (LC-MS/MS) analysis. For identification of *S*-bacillithiolated and itaconated Cys-peptides, NEM-alkylated protein extracts were prepared from *S. aureus* COL after exposure to 13 mM itaconic acid for 30 min as described above for the Western blot analysis. The protein extracts of the 3 biological replicates were separated using a short 12% SDS-PAGE and stained with Coomassie blue. The lanes of each sample were cut into 5 gel fractions, which were subjected to tryptic in-gel digestion as described [32,50]. For Orbitrap LC-MS/MS analysis, the peptides were dissolved in 30 μl of 0.05% trifluoroacetic acid (TFA) with 5% acetonitrile, diluted 1:30, and 6 μl were analyzed by an Ultimate 3000 reverse-phase capillary nano liquid chromatography system connected to an Orbitrap Q Exactive HF mass spectrometer (Thermo Fisher Scientific) as described [50]. Samples were injected and concentrated on a trap column (PepMap100C_{18}, 3 μm, 100 Å, 75 μM i.d. x 2 cm; Thermo Fisher Scientific) equilibrated with 0.05% TFA in water. After switching the trap column in-line, LC separations were performed on a reverse-phase column (Acclaim PepMap100C_{18}, 2 μm, 100 Å, 75 μm i.d. x 25 cm, Thermo Fisher Scientific) at an eluent flow rate of 300 nl/min. The mobile phase A contained 0.1% formic acid in water, and the mobile phase B contained 0.1% formic acid in 80% acetonitrile/20% water. The column was pre-equilibrated with 5% mobile phase B, followed by an increase of 5–44% mobile phase B in 100 min. The mass spectra were acquired in a data-dependent mode utilizing a single MS survey scan (*m/z* 300 - 1,650) with a resolution of 60,000, and MS/MS scans of the 15 most intense precursor ions with a resolution of 15,000 and a normalized collision energy of 27. The isolation window of the quadrupole was set to 1.4 *m/z*. The dynamic exclusion time was set to 20 s and automatic gain control was set to $3x10^6$ and $1x10^5$ for MS and MS/MS scans, respectively.

Data processing and identification of proteins with *S*-bacillithiolations and *S*-itaconations was performed using the Mascot software package (Mascot Server version 2.7, Mascot Distiller version 2.8, Mascot Daemon version 2.7, Matrix Science) as described [50]. Processed spectra were searched against the *S. aureus* COL database downloaded from Uniprot (2,680 sequences, Proteome ID UP000000530, last modified on 19th December 2022) [51]. A maximum of two missed cleavages was allowed and the mass tolerance of precursor and sequence ions was set to 10 ppm and 0.02 Da, respectively. Methionine oxidation (Met+15.994915 Da), cysteine alkylation by NEM (Cys+ 125.047679 Da), cysteine *S*-bacillithiolation (Cys+ 396.083866 Da for $C_{13}H_{20}N_2O_{10}S_1$) with the malate neutral loss (Cys+ 134.021523 for $C_4H_6O_5$) and cysteine *S*-itaconation (Cys+ 130.026609 for $C_5H_6O_4$) were set as variable modifications. A significance threshold of 0.05 was used as a cut-off and the MS/MS spectra of the identified peptides with the post-translational thiol-modifications were manually approved. The shotgun MS data have been deposited at the ProteomeExchange Consortium via the PRIDE [52] partner repository with the dataset identifier PXD042939 and 10.6019/PXD042939.

Extracellular metabolome analysis. The extracellular metabolome samples were prepared from 3 biological replicate experiments. *S. aureus* COL was grown in RPMI until an OD_{500} of 0.5, followed by exposure to 13 mM itaconic acid. The extracellular metabolome samples were harvested directly after inoculation (t0) and from itaconic acid-treated and untreated cultures at the time points 0 (OD_{500} of 0.5), 30, 60 and 120 min as described previously [53]. At every sampling time point, starting at t0 directly after inoculation, 2 ml cell suspension was filtered using a syringe and a 0.2-μm-pore-size filter (Sarstedt) to obtain sterile extracellular metabolite samples of the bacterial cultures. All filtrates were collected in liquid nitrogen and subsequently stored at −80 °C before measurement. The ^{1}H nuclear magnetic resonance (^{1}H-NMR) analysis of the extracellular metabolite samples was performed according to previous protocols [54,55].

Intracellular metabolome analysis. For the intracellular

metabolome analysis, *S. aureus* COL was grown in RPMI to an OD_{500} of 0.5, followed by the exposure to 13 mM itaconic acid. The cytoplasmic metabolite samples were collected from itaconic acid-treated and untreated cultures at the time points 0 (=OD_{500} of 0.5), 30, 60 and 120 min according to previous protocols [53]. At every sampling time point, 10 OD units of the bacterial culture (equivalent to 10 ml culture at an OD_{500} of 1.0) were harvested by using the vacuum-dependent fast-filtration approach as described [53]. The filter with the bacterial cells was washed twice with 12.5 ml of an ice-cold (0–4 °C) isotonic 135 mM NaCl solution, followed by its transfer to a 50 ml-falcon tube containing 2.5 ml of the ice-cold extraction solution (60% ethanol [wt/vol]). The tube was closed, shortly mixed, quick-frozen in liquid nitrogen and the frozen samples were stored at −80 °C until measurements [53]. The dried samples were derivatized and the intracellular metabolites measured using gas chromatography-mass spectrometry (GC-MS) analysis as previously described [53,55]. A GC system (7890B, Agilent) with an autosampler, an injector (model G4513A), and a coupled mass selective detector (model 5977B MSD) (Agilent) were used for intracellular metabolite measurements as described [53,55].

3. Results

The growth-inhibitory concentration of itaconic acid stress depends on the pH of the growth medium. First, we monitored the growth of *S. aureus* COL in LB and RPMI medium upon exposure to increasing concentrations of itaconic acid during the log phase to determine the sublethal dose, which reduces the growth rate half-maximal without killing effects (Fig. 1A, C). In addition, the acidification of the growth medium was monitored after treatment of *S. aureus* with itaconic acid (Fig. 1B, D). Interestingly, *S. aureus* was much more sensitive to itaconic acid when grown in LB compared to RPMI. While the sublethal concentration was determined as 13 mM itaconic acid in RPMI, a much lower dose of 3 mM itaconic acid affected the growth of *S. aureus* in LB (Fig. 1A, C). This was unexpected, since we anticipated that the rich LB quenches the electrophilic itaconic acid more than the defined RPMI medium according to previous studies with oxidants, such as HOCl [36,41]. However, itaconic acid is a weak dicarboxylic acid (pKa of 3.85 and 5.45) [23], leading to differential acidification of both growth media, depending on the starting pH of the bacterial culture as shown previously for itaconic acid [24] and other weak acids [56]. While the external pH of the RPMI-grown culture dropped from 8.5 to 5.5 after exposure to 13 mM itaconic acid, the initial pH of the LB culture was much lower with 6.5, and the addition of 3 mM itaconic acid was sufficient for the acidification to pH 5.5, limiting bacterial growth (Fig. 1B, D). Further growth experiments of RPMI-grown cells at the starting pH of 7.5 and 6.5 decreased the growth rate-reducing itaconic acid concentration to 10 and 7 mM, respectively (Fig. S1). Thus, the growth-inhibitory concentration and antimicrobial activity was dependent on the starting pH of the bacterial culture and correlated with the pH decrease to 5.5 upon acidification by itaconic acid, and was not dependent on the different ROS/RES quenching effects of both growth media.

Itaconic acid stress causes an acid and oxidative stress response in the *S. aureus* transcriptome. Next, we investigated the specific stress responses and gene expression profile of *S. aureus* COL after exposure to 13 mM itaconic acid in the RPMI-grown culture using RNA-seq transcriptomics. In agreement with previous stress experiments, we have chosen the growth in RPMI for itaconic acid stress, since this cell culture medium mimics infection conditions and is more physiologically relevant for *S. aureus* [57]. The RNA-seq transcriptome analysis was performed from 3 biological replicates of *S. aureus* COL harvested before and after 30 min of exposure to 13 mM itaconic acid stress. For significant fold-changes in gene expression, the M-value cut-off (log2-fold change itaconic acid/control) of ≥1 and ≤-1 was applied, resulting in 319 and 358 transcripts, which were significantly >2-fold up- and downregulated, respectively by itaconic acid (Fig. 2, Tables S3 and S4).

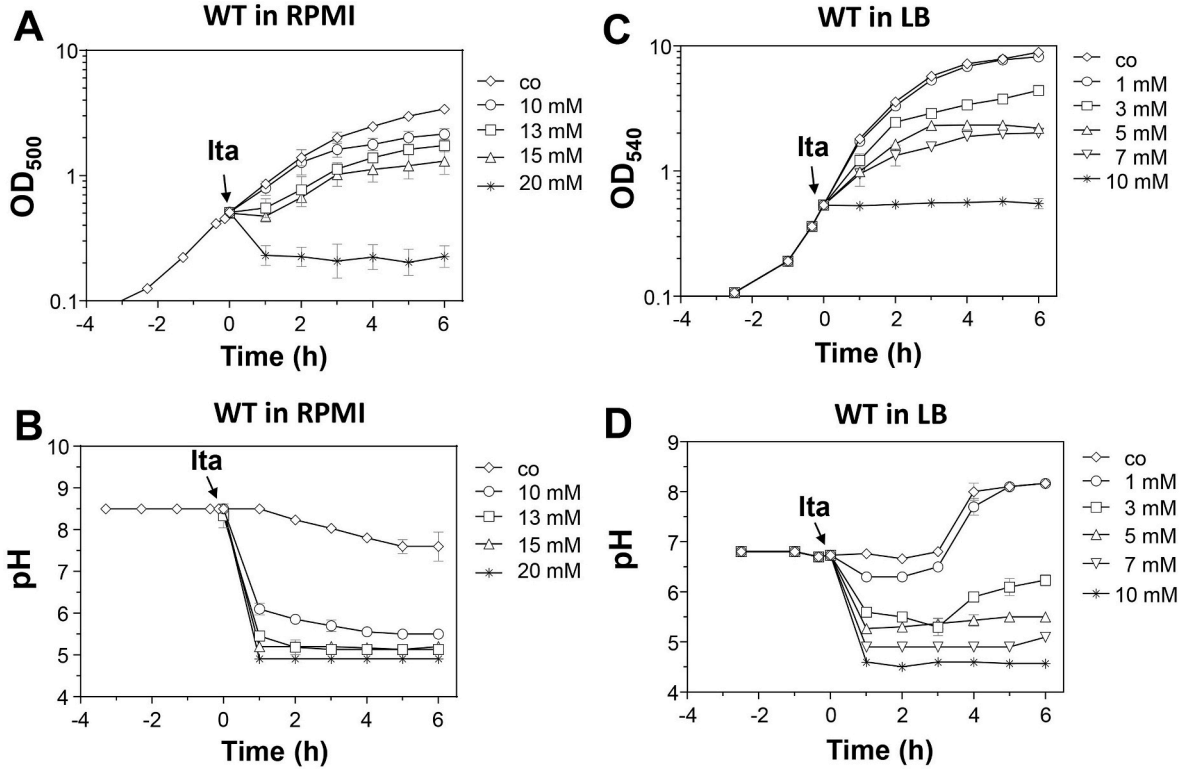

Fig. 1. Susceptibility and extracellular acidification of *S. aureus* after treatment with itaconic acid in RPMI and LB medium. The growth curves (A, C) and extracellular pH changes (B, D) of *S. aureus* COL were monitored in RPMI (A, B) and LB medium (C, D) after exposure to increasing doses of itaconic acid stress during the log phase at an OD_{500} and OD_{540} of 0.5, respectively. The results are from each 3 biological replicates. Error bars represent the standard deviation (SD).

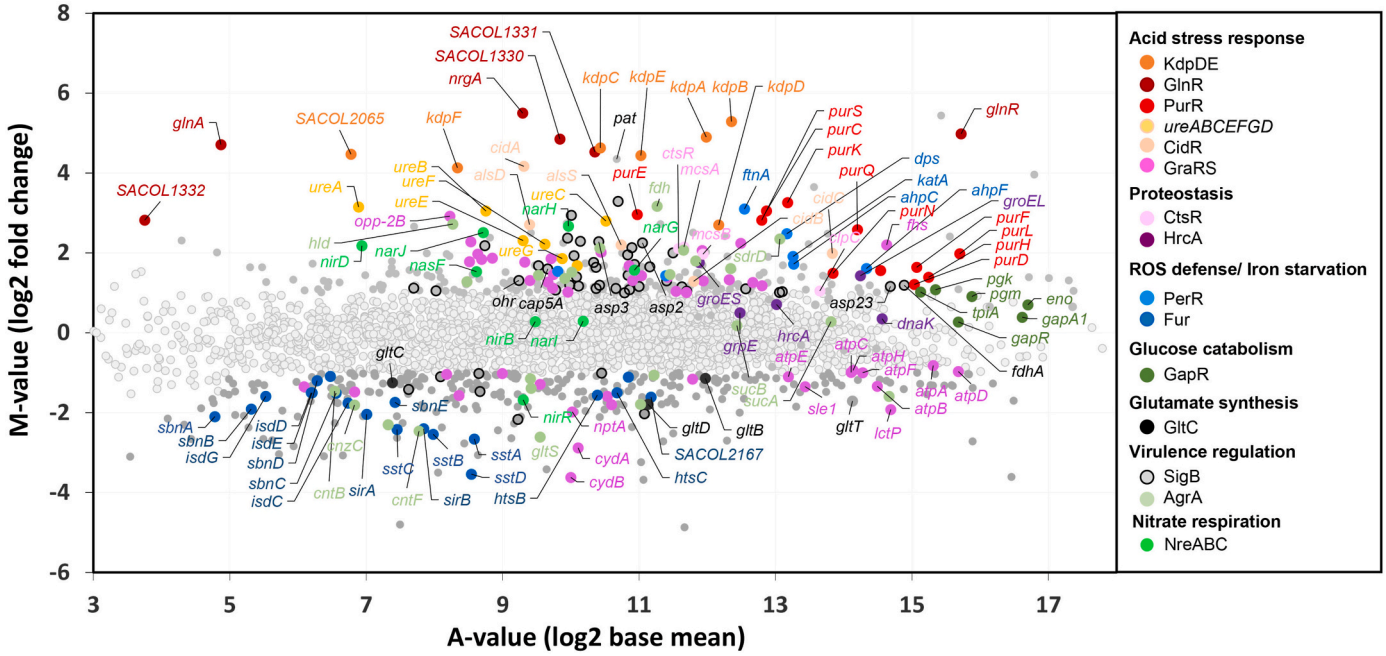

Fig. 2. RNA-seq transcriptomics of *S. aureus* COL after itaconic acid stress indicates an acid and oxidative stress response. For RNA-seq transcriptome profiling, *S. aureus* COL grown in RPMI to an OD_{500} of 0.5 was treated with sub-lethal 13 mM itaconic acid for 30 min. The gene expression profile in response to itaconic acid stress is shown as ratio/intensity scatter plot (M/A-plot), which is based on the differential gene expression analysis using DeSeq2. Light gray symbols denote transcripts with no fold-changes ($p > 0.05$). Dark gray symbols indicate significantly induced and repressed transcripts (M-value $\geq$1.0 or ≤ -1.0; $p \leq 0.01$), which are color-coded according to their regulons. All annotated regulons were functionally classified into acid stress responses (KdpDE, GlnR, PurR, CidR and GraRS regulons and the *ureABCEFGD* operon), proteostasis (CtsR, HrcA), ROS defense and iron starvation (PerR, Fur), glycolysis (GapR), glutamate synthase (GltC), virulence regulons (SigB, AgrA) and nitrate respiration (NreABC). The transcriptome analysis was performed from 3 biological replicates. The RNA-seq expression data of all differentially transcribed genes after itaconic acid stress and their regulon classifications are listed in Tables S3 and S4.

Among the top scorers were the 6.5–45-fold upregulated KdpDE and GlnR regulons under itaconic acid stress. The two-component system KdpDE controls the potassium transporting ATPase KdpABCF (17.5–39-fold), which is involved in the high-affinity uptake of K^+ as counter ion of protons upon acidification provoked by itaconic acid (Fig. 2, Tables S3 and S4). Transcriptional induction of the large *kdpABCF* operon upon itaconic acid stress was confirmed using Northern blots (Fig. S2). The *kdpABCF* operon has been shown to respond to osmotic stress and mild acid stress in *S. aureus* [58,59]. The nitrogen starvation-responsive GlnR regulon includes the glutamine synthase GlnA (FemC) (34-fold), three small hypothetical proteins encoded downstream of the *glnRA* operon (SACOL1330-31-32) and an ammonium transporter NrgA (45-fold) with high affinity for ammonium uptake, indicating that itaconic acid induces ammonium limitation in *S. aureus* [60]. During acidification, the membrane-permeable ammonia is protonated to ammonium ions, which are charged and not membrane diffusible [60]. Thus, despite the presence of 2 mM glutamine in the growth medium, itaconic acid leads to ammonium limitation, resulting in induction of the GlnR regulon. The acid stress response is confirmed by the 3–8.9-fold upregulation of the *ureABCEFGD* operon, which encodes the urease subunits catalyzing the degradation of urea to ammonium for regeneration of the pH homeostasis [61]. Northern blot analyses validated the upregulation of the *ureABCEFGD* operon under itaconic acid stress (Fig. S2). Furthermore, the cell death and lysis controlling CidR regulon was significantly upregulated, including the *cidABC* (4-18-fold) and *alsSD* operons (4.5–6.5-fold) (Fig. 2, Tables S3 and S4). Transcriptional induction of the *alsSD* operon under itaconic acid was validated using Northern blot analysis (Fig. S2). The *alsSD* operon encodes the α-acetolactate synthase/decarboxylase pathway, which consumes protons to produce the neutral product acetoin from pyruvate to restore pH homeostasis [56,62,63]. The pyruvate decarboxylase CidC generates acetate, which was previously linked to cell death upon acid stress [63]. In addition, itaconic acid leads to strong upregulation of the PurR regulon for purine biosynthesis (2–9.6-fold), whereas transcription of the PyrR regulon for pyrimidine biosynthesis was only weakly induced (1.6-2-fold). Because glutamine and ammonium are required for nucleotide biosynthesis, the N-limitation affects purine and pyrimidine biosynthesis, leading to induction of the *purEKCSQLFMNHD* and *uraA-pyrBC-carAB-pyrFE-SACOL1218* operons. Acidification further leads to DNA damage, which requires new nucleotide and DNA biosynthesis.

Itaconic acid stress leads to ROS formation, which is indicated by the strong 2–8.5-fold induction of the genes belonging to the peroxide-inducible PerR regulon, encoding the catalase (*katA*), the peroxiredoxins (*ahpCF, bcp, tpx*), and the iron-storage proteins (*dps, ftnA*) [30]. However, itaconic acid elicits only a weak induction of the quinone-sensing QsrR and MhqR regulons (2–6.5-fold), which were previously induced by quinones and oxidants in *S. aureus* (Fig. 2, Tables S3 and S4) [50,64]. In agreement with acid and oxidative stress-induced protein damage, the CtsR and HrcA regulons for protein quality control (ClpP, ClpC, ClpB proteases and DnaK-GroESL chaperones) were 1.5–4.5-fold upregulated by itaconic acid in *S. aureus*. Among the large GraRS cell wall stress regulon, which senses host defense peptides under acidic conditions (pH 5.5) in the phagolysosome of macrophages [65], the *opp-2FDCB* operon for peptide transport (2.5–7.5-fold) and the glycine/betaine uptake *opuCD-CC-CB-CA* operon (2.5-4-fold) were upregulated. In contrast, the staphylococcal respiratory response two-component system (SrrAB)-dependent *cydAB* and *qoxABCD* operons, encoding the cytochrome *bd* and *aa_3* ubiquinol oxidases for aerobic respiration were 0.08–0.75-fold downregulated, suggesting the inhibition of aerobic respiration. Moreover, the nitric oxide-responsive NreABC regulon, which includes the nitrate and nitrite reductase operons (*narIJHG* and *nirRBD-nasF*) was induced (2.9–6.4-fold), pointing to the switch to anaerobic respiration upon itaconic acid stress [66]. The ATP synthase-encoding *atpCDGAHFEBI* operon was 0.4–0.5-fold downregulated indicating a reduced electron

flow through the respiratory chain. However, the Rex regulon including fermentation genes, such as the *pflAB* operon and the *ldh1* gene encoding the pyruvate formate-lyase and the lactate dehydrogenase, respectively, were 0.28–0.34-fold repressed. Of note, the iron starvation-inducible Fur regulon was strongly 0.1–0.5-fold downregulated, supporting a decreased iron uptake under ROS-producing conditions to prevent the Fenton chemistry. In addition, the virulence factor controlling stress and starvation sigma factor B (SigB) and accessory gene regulator A (AgrA) regulons were differentially expressed under itaconic acid stress (Fig. 2, Tables S3 and S4). Overall, the RNA-seq transcriptome analysis indicates that *S. aureus* encounters strong acid and oxidative stress as well as protein damage and changes in energy metabolism under itaconic acid stress.

Itaconic acid leads to higher acetoin and pyruvate secretion and enhanced uptake of several amino acids in the intracellular metabolome. The transcriptomic signature revealed that itaconic acid causes the strong induction of the CidR-controlled *alsSD* operon for acetoin production to regenerate pH homeostasis. In addition, the pathways for central glucose catabolism, including the glycolytic GapR regulon, the *pta* and *ackA* operons for overflow metabolism, the pyruvate dehydrogenase encoding *pdhABCD* operon and some TCA cycle genes were weakly upregulated upon itaconic acid stress in the transcriptome (Fig. 2, Tables S3 and S4). Thus, we used GC-MS and ^{1}H-NMR spectroscopic analysis to investigate the effect of itaconic acid on the changes of the intracellular and extracellular metabolites of the glycolysis, TCA cycle, overflow metabolism, fermentation and amino acid metabolism in *S. aureus* (Figs. 3–5, Tables S5–S6). Itaconic acid treatment had no effect on glucose consumption and utilization, since the level of glucose decreased similar within 120 min after t0 in the extra- and intracellular metabolomes of itaconic acid-treated and untreated cells (Fig. 3A, Tables S5–S6). While secretion of formate and acetate was significantly decreased in the exometabolome of *S. aureus* upon challenge with itaconic acid, acetoin was strongly enhanced supporting that the *alsSD* operon plays a major role to restore pH homeostasis (Fig. 3B–D). However, we did not detect 2,3-butandiol secretion in the exometabolome although the transcription of the acetoin reductase-encoding *butA* gene was induced by itaconic acid (Fig. 2, Tables S3–S5). Consistent with the glucose levels, the intracellular metabolites of the glycolysis and TCA cycle declined within 120 min after t0 with no differences between itaconic acid-treated and control samples (Fig. 3F, H; Table S6). However, significantly higher levels of pyruvate and fumarate were secreted in the extracellular metabolome of itaconic acid-treated cells, suggesting an enhanced glycolytic and TCA cycle activity (Fig. 3E, G, Table S5).

In addition, the majority of amino acids declined in the extracellular metabolome of *S. aureus* within 120 min after t0 (Table S5). Itaconic acid caused a stronger decrease of glycine, threonine, aspartate, valine, leucine, methionine and glutamate, while the extracellular levels of proline and histidine are increased compared to the control (Fig. 4A, C, D, E, F, H, I, J, K; Table S5). Consistent with their extracellular depletion, the intracellular levels of threonine, aspartate, valine, leucine and methionine were strongly increased under itaconic acid stress, supporting their enhanced uptake (Fig. 5C, D, F, G, L; Table S6). In addition, the intracellular levels of lysine, histidine, alanine, β-alanine, cysteine and isoleucine were strongly elevated by itaconic acid, despite of a limited extracellular decrease compared to the control (Table S6; Fig. 5B, E, H, I, J, K). The amino acids lysine, histidine, aspartate, proline and alanine are the dominant amino acids, accumulating inside *S. aureus* cells during the course of glucose starvation in the stationary phase [67]. Lysine is synthesized from aspartate, which is used as central building

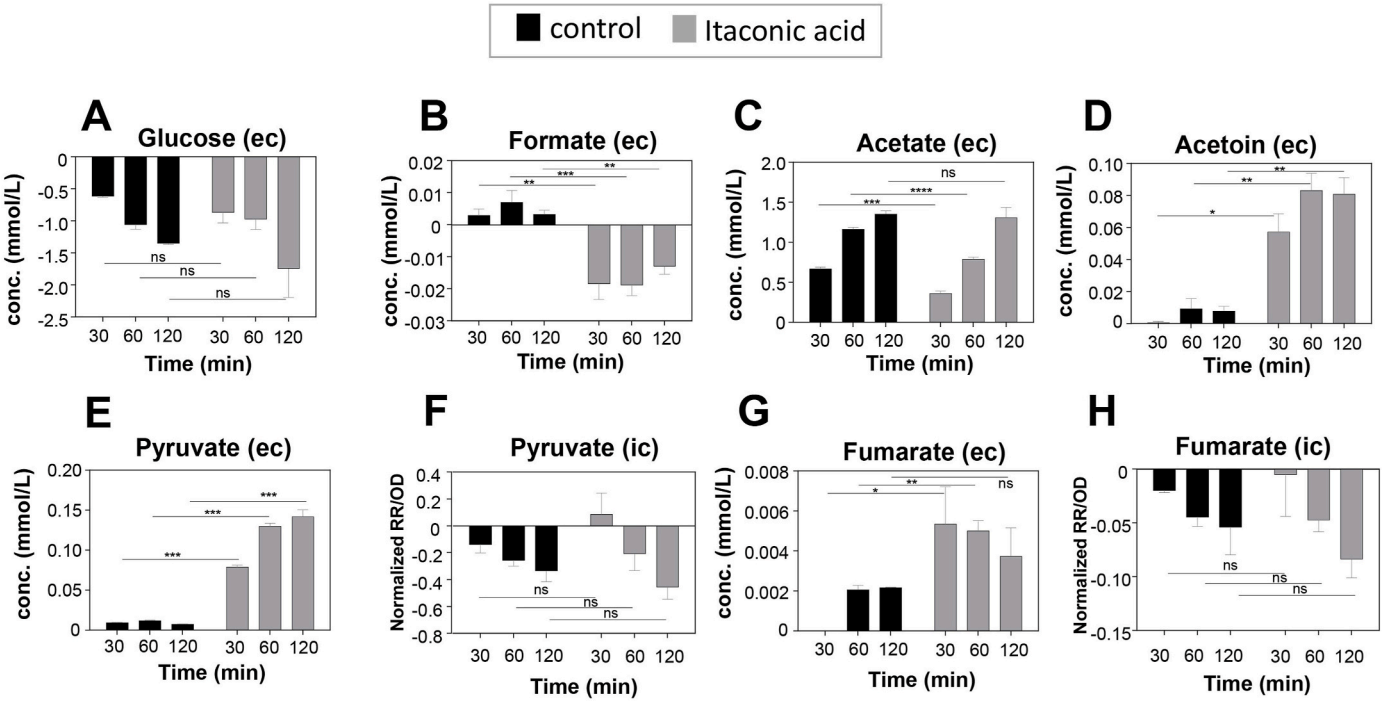

Fig. 3. Itaconic acid leads to decreased formate and acetate secretion and enhanced levels of acetoin, pyruvate and fumarate in the exometabolome of *S. aureus*. *S. aureus* COL grown in RPMI to an OD_{500} of 0.5 was exposed to 13 mM itaconic acid. The exometabolome analysis was performed from samples harvested at time points 0, 30, 60 and 120 min with or without the exposure to 13 mM itaconic acid. The concentrations of the extracellular metabolites were calculated in relation to the control time point at an OD_{500} of 0.5, which was set to 0. The intracellular metabolites pyruvate and fumarate were calculated as relative responses (RR), which are the areas of the metabolites versus the areas of internal standards (ISTD). The RR values were normalized to the control time point at an OD_{500} of 0.5, which was set to 0. Mean mean values of the RR/OD_{500} ratios of 3 biological replicates were presented, except for the itaconic acid stress sample at 120 min, where only two replicates could be used due to the limited size of the ISTD in the 3rd replicate. Error bars represent the standard deviation. The statistics was calculated using a Student's unpaired two-tailed *t*-test by the graph prism software. Symbols are: $^{ns}p > 0.05$, $^{*}p < 0.05$, $^{**}p < 0.01$, $^{***}p < 0.005$ and $^{****}p < 0.0001$. Abbreviations: ec, extracellular; ic, intracellular.

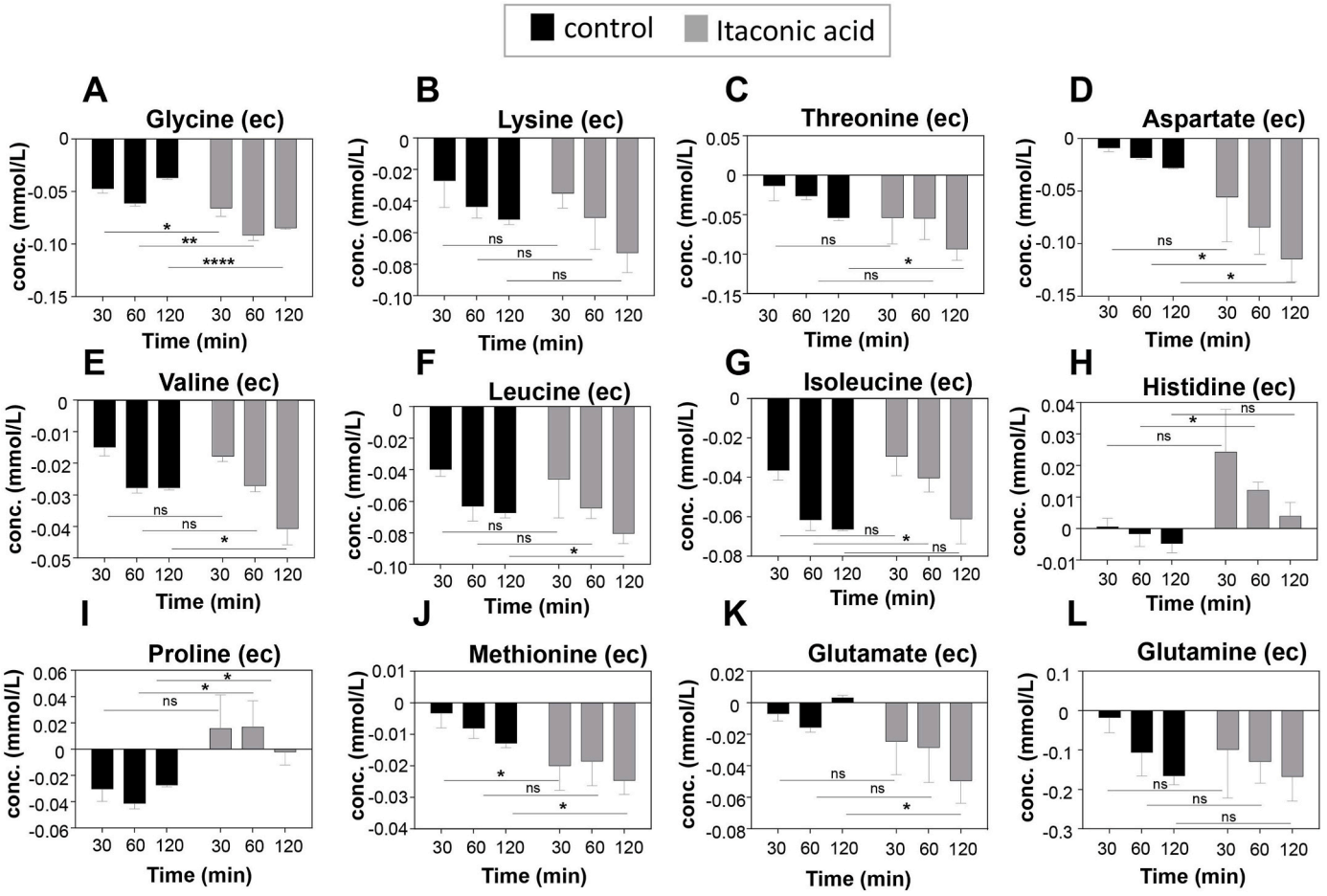

Fig. 4. Itaconic acid causes stronger depletion of glycine, threonine, aspartate, valine, leucine, methionine and glutamate in the extracellular metabolome of *S. aureus*, while proline and histidine levels are increased compared to the control. *S. aureus* COL grown in RPMI to an OD_{500} of 0.5 was exposed to 13 mM itaconic acid. The exometabolome analysis was performed from samples harvested at time points 0, 30, 60 and 120 min with or without the exposure to 13 mM itaconic acid. The concentrations of the extracellular metabolites were calculated in relation to the control time point at an OD_{500} of 0.5, which was set to 0. Mean values 3 biological replicates are presented. Error bars represent the standard deviation. The statistics was calculated using a Student's unpaired two-tailed *t*-test by the graph prism software. Symbols are: $^{ns}p > 0.05$, $^{*}p < 0.05$, $^{**}p < 0.01$, $^{***}p < 0.005$ and $^{****}p < 0.0001$. Abbreviations: ec, extracellular.

block for metabolites of many pathways, including the gluconeogenesis, the pentose-phosphate pathway, the nucleotide biosynthesis and other amino acid biosynthesis pathways (alanine, asparagine) [68]. The high uptake of the basic amino acid lysine, which contains an ammonium side chain, was shown to be driven by the membrane potential in exchange of potassium to restore the pH homeostasis upon acid stress [69]. Similarly, the increased level of the basic histidine might contribute to pH homeostasis. Cysteine is synthesized from threonine via glycine and serine. While threonine uptake was enhanced by itaconic acid (Fig. 5C), the intracellular glycine and serine levels were depleted within 120 min after t0 (Fig. 5A; Table S6), suggesting that they have been used-up for cysteine biosynthesis. Enhanced cysteine levels are required for the synthesis of the LMW thiol BSH to regenerate the redox homeostasis upon itaconic acid stress. Furthermore, the amino acids glutamate, glutamine and proline showed a similar time-dependent decline in the intracellular metabolome of itaconic acid-treated and control cells (Fig. 5M, N, O), whereas the level of proline was elevated in the extracellular medium (Fig. 4I). Glutamate is an amino group donor and the precursor for glutamine synthesis via GlnA, which is upregulated under itaconic acid stress due to ammonium starvation (Fig. 2). Glutamine and ammonium are important nitrogen donors of *S. aureus* and have been shown to promote growth [70]. Thus, the decline of the cellular glutamine pool probably limits the growth of *S. aureus* in RPMI medium. Taken together, the intra- and extracellular metabolome analyses revealed an enhanced secretion of pyruvate, fumarate and acetoin as well as increased intracellular amounts of several amino acids, including lysine, threonine, aspartate, histidine, alanine, valine, leucine, cysteine and methionine, which might be required to restore pH and redox homeostasis upon itaconic acid stress in *S. aureus*.

Urea supplementation rescues the growth of itaconic acid-treated cells, whereas glutamine does not improve the growth. Our results showed that acidification by itaconic acid leads to the induction of the urease and glutamine synthetase, indicating ammonium generation and nitrogen limitation, respectively. Thus, we analyzed whether supply with the extracellular nitrogen donors urea and glutamine could restore the growth and neutralize the pH of the itaconic acid-treated culture (Fig. 6). Indeed, the supplementation of the growth medium with 20 mM urea restored the growth of the itaconic acid-treated culture to WT level, leading to neutralization of the external pH within few hours (Fig. 6A and B). However, an excess of 20 mM glutamine did not improve the growth and the pH remained acidic (Fig. 6C and D). Thus, we conclude that the itaconic acid effect in *S. aureus* is predominated by the imposed acid stress, which can be neutralized by urea as ammonium source. In contrast, the ammonium starvation effect cannot be compensated by higher glutamine levels and requires the GlnR-controlled high-affinity ammonium transporter NrgA, since protonated ammonium cannot diffuse through the membrane [60]. We were further interested whether the acid stress effect of itaconic acid would be similar for the related dicarboxylic acid succinic acid. The sub-lethal dose of succinic acid was determined as 13 mM

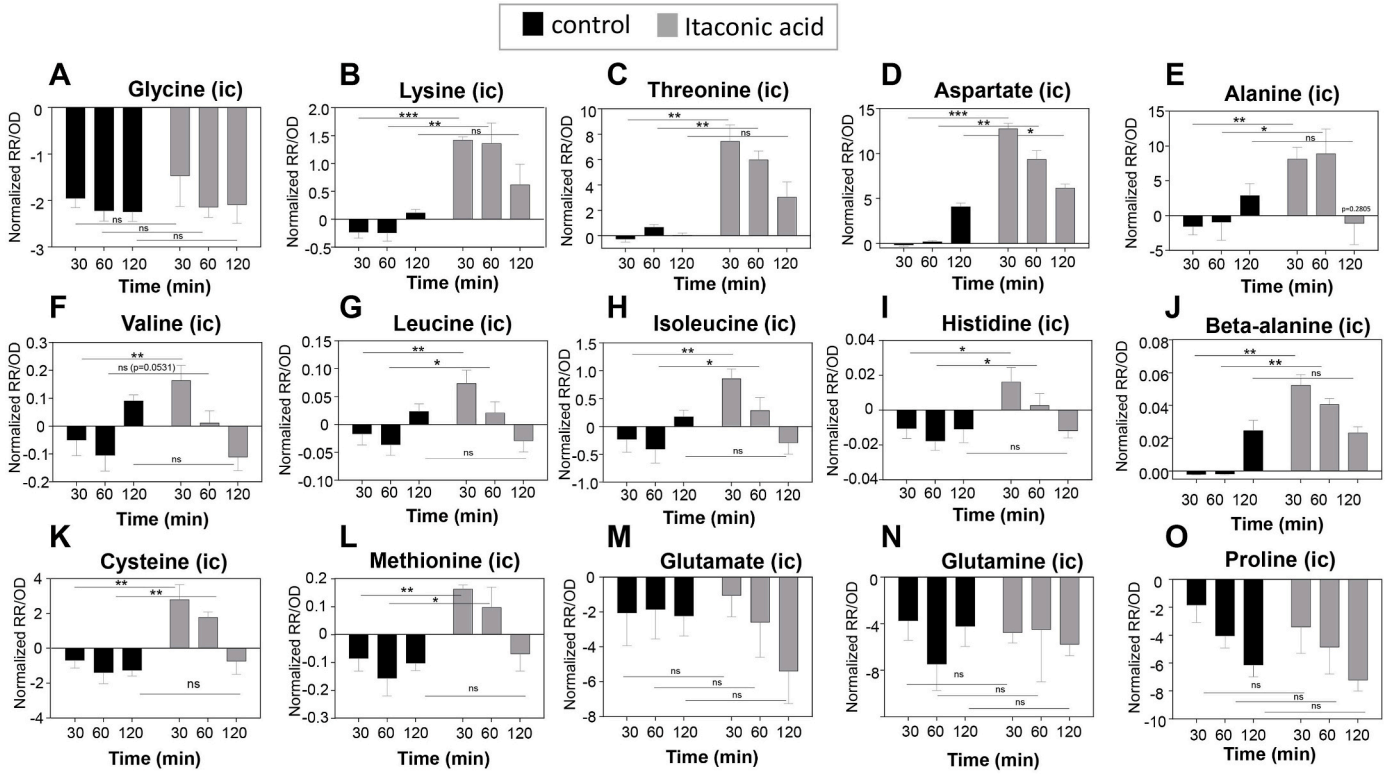

Fig. 5. The amino acids lysine, threonine, aspartate, alanine, β-alanine, histidine, cysteine, methionine, valine, isoleucine and leucine are increased in the intracellular metabolome after itaconic acid stress. *S. aureus* COL grown in RPMI to an OD_{500} of 0.5 was exposed to 13 mM itaconic acid. For intracellular metabolome analysis, *S. aureus* cultures were harvested at 10 OD units at the time points 0, 30, 60 and 120 min with or without the exposure to 13 mM itaconic acid. The intracellular metabolites were calculated as relative responses (RR), which are the areas of the metabolites versus the areas of internal standards (ISTD). The RR values were normalized to the control time point at an OD_{500} of 0.5, which was set to 0. Mean mean values of the RR/OD_{500} ratios of 3 biological replicates were presented, except for the itaconic acid stress sample at 120 min, where only two replicates could be used due to the limited size of the ISTD in the 3rd replicate. Error bars represent the standard deviation. The statistics was calculated using a Student's unpaired two-tailed *t*-test by the graph prism software. Symbols are: $^{ns}p > 0.05$, $^{*}p < 0.05$, $^{**}p < 0.01$, $^{***}p < 0.001$ and $^{****}p < 0.0001$.
Abbreviations: ic, intracellular.

(Fig. S3A), which led to the same acidification and pH decrease of 5.5 of the growth medium as revealed for itaconic acid (Fig. S3B, Fig. 6E and F). In addition, urea supplementation restored the growth of the succinic acid-treated culture and resulted in the neutralization of the external pH (Fig. 6E and F), pointing to similar acid stress mechanisms provoked by itaconic acid and succinic acid in *S. aureus*.

Urea supplementation abolishes the itaconic acid-induced GlnR-dependent ammonium limitation. To investigate whether the acid stress response by itaconic acid is abolished by urea supplementation, but not by enhanced glutamine supply, we analyzed the transcription of the GlnR regulon in the urea or glutamine supplemented RPMI medium after itaconic acid stress. The Northern blot results showed a strong induction of the *glnRA* operon by itaconic acid stress in *S. aureus* grown without urea (Fig. 7A and B). While urea supplementation significantly reduced the transcription of the *glnRA* operon, additional glutamine supply did not affect the level of *glnRA* transcription. These results support that itaconic acid acts as weak acid to provoke ammonium limitation in *S. aureus* due to the acidification of the medium, which prevents the uptake of protonated ammonium required for neutralization of the intracellular pH [60].

Itaconic acid causes an oxidative stress response and widespread protein *S*-bacillithiolation in *S. aureus*. Apart from acid stress, itaconic acid caused an oxidative stress response as revealed by the induction of the peroxide-inducible PerR regulon, including the genes encoding the catalase KatA and the peroxidredoxin AhpCF (Fig. 2, Tables S3 and S4). To monitor whether the oxidative stress response is dependent on the acidification or the electrophile mode of action of itaconic acid, we analyzed the transcription of *katA* and *ahpCF* after itaconic acid in the urea-supplemented medium. While transcription of *katA* and *ahpCF* was strongly upregulated in *S. aureus* exposed to itaconic acid in urea-free RPMI medium, both transcripts showed lower expression in the urea medium, although the differences were less significant as for the *glnRA* operon induction (Fig. 7A, C, D). This indicates that pH neutralization by urea supplementation can only partially reduce ROS formation by itaconic acid due to its electrophile mode of action, which cannot be compensated by urea buffering. In addition, we added the ROS scavenger N-acetyl cysteine (NAC) to see whether the growth is improved after itaconic acid exposure. However, addition of 1.25 and 2.5 mM NAC further decreased the growth after itaconic acid stress (Fig. S4), indicating that acid stress is the main contributor of the antimicrobial mode of action, independent on the ROS induction.

To investigate the oxidative mode of action of itaconic acid, we analyzed the extent of reversible protein *S*-bacillithiolation in *S. aureus* using non-reducing BSH-specific Western blot analysis and Orbitrap Q Exactive LC-MS/MS analysis. Previously, we detected strong *S*-bacillithiolations and increased protein thiol-oxidation after exposure to the strong oxidant HOCl in *S. aureus* USA300 [34]. The glyceraldehyde dehydrogenase GapA was the most abundant target for *S*-bacillithiolation in HOCl-stressed *S. aureus* cells [34]. Thus, we used a protein extract of HOCl-stressed *S. aureus* cells as positive control for *S*-bacillithiolation confirming GapA as major band (Fig. 8A). Interestingly, itaconic acid-treated cells showed strongly enhanced *S*-bacillithiolations in the BSH-Western blots, but the pattern was different compared to that of HOCl-treated cells (Fig. 8A). The profile of itaconic acid-induced *S*-bacillithiolations was not observed in the *bshA* mutant and could be reversed with DTT (Fig. 8A, B), supporting that itaconic acid provoked

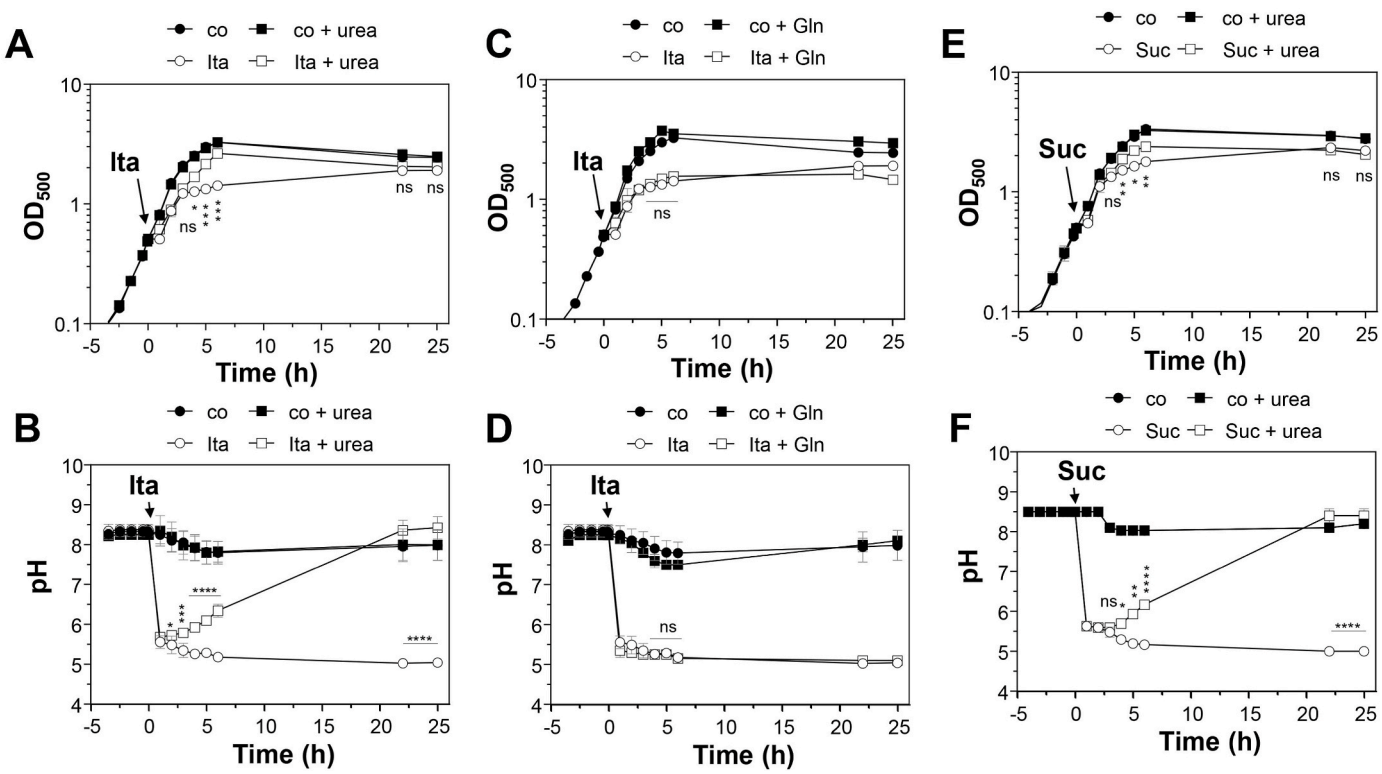

Fig. 6. Urea supplementation in RPMI protects *S. aureus* COL against itaconic acid and succinic acid stress. For growth curves, the *S. aureus* COL WT was grown in RPMI with or without 20 mM urea or 20 mM glutamine until an OD_{500} of 0.5 and treated with 13 mM itaconic acid **(A, C)** or 13 mM succinic acid **(E)**. Extracellular pH of the *S. aureus* culture was monitored along the growth **(B, D, F)**. Mean values and SD of 3–4 biological replicates are presented. The statistics for "Ita" versus "Ita + urea" and for "Suc" versus "Suc + urea" were calculated using a Student's unpaired two-tailed *t*-test by the graph prism software. Symbols are: $^{ns}p > 0.05$, $*p \leq 0.05$, $**p \leq 0.01$, $***p \leq 0.001$ and $****p \leq 0.0001$.

oxidative stress by inducing protein *S*-bacillithiolations. Furthermore, we used the BSH-specific Western blots to analyze whether succinic acid causes *S*-bacillithiolations in the proteome. Indeed, we detected strongly increased protein *S*-bacillithiolations after exposure to succinic acid in *S. aureus* COL, which were absent in the *bshA* mutant and reversible with DTT (Fig. 8C, D). Altogether, our results showed that itaconic acid caused an oxidative stress response indicated by the induction of the PerR-dependent antioxidant response and an enhanced protein *S*-bacillithiolation.

In addition, Orbitrap Q Exactive LC-MS/MS analysis was applied to identify the targets of *S*-bacillithiolations in itaconic acid-stressed cells (Table 1, Table S7). In total, 15 proteins were modified by *S*-bacillithiolation in *S. aureus* COL after itaconic acid stress in at least 2 out of 3 biological replicates (Table 1, Table S7). Among the proteins with *S*-bacillithiolations were the glycolytic GapA and the inosine-5-monophosphate dehydrogenase GuaB, which are the most HOCl-sensitive targets, exhibiting 29% increased thiol-oxidation in HOCl-stressed cells [34]. However, the remaining 13 proteins were not detected as BSH-modified under HOCl stress [34]. Among the redox-sensitive *S*-bacillithiolated proteins in itaconic acid-stressed cells were the monothiol bacilliredoxin BrxC, the thioredoxin protein SACOL1992 and the glyoxalase-III HchA, which were modified by BSH at their active site Cys residues, including Cys63 of SACOL1992, Cys30 of BrxC and Cys214 of HchA (Table 1, Table S7). Many targets for *S*-bacillithiolations function in the central carbon catabolism, including the glycolysis (GapA, the transaldolase Tal and the triosephosphate isomerase TpiA), overflow metabolism (phosphate acetyl transferase Pta), the pyruvate dehydrogenase complex (PdhC, PdhD) and the TCA cycle (malate-quinone oxidoreductase SACOL2623), which showed elevated expression in the transcriptome (Tables S3 and S4). Interestingly, the glutamine synthetase GlnA and glutamate dehydrogenase GluD were *S*-bacillithiolated, which are central for the acid stress response, since *glnA* transcription was strongly upregulated in the transcriptome due to ammonium limitation, while GluD might contribute to ammonium production from glutamate. Thus, the *S*-bacillithiolation profile includes important targets, which regulate the cellular metabolism and pH homeostasis upon itaconic acid stress, which might be protected against irreversible oxidation by *S*-bacillithiolation.

Itaconic acid acts as electrophile and causes protein *S*-itaconation in the proteome. Itaconate has been shown to react as electrophile via the *S*-alkylation chemistry with protein thiols, leading to widespread itaconation in the proteome of macrophages and bacteria [20,21]. Thus, we searched our shotgun proteome dataset for itaconation sites. The Mascot search results revealed 23 proteins, which were modified by itaconation in 2 out of 3 biological replicates, as revealed by a mass shift of 130 Da at Cys residues (Table 2, Table S8). There was only a limited overlap between the targets modified by *S*-itaconations and *S*-bacillithiolation in *S. aureus* cells, including GuaB, the Mn-independent inorganic pyrophosphatase PpaC and the ribosomal protein RpmJ, which were *S*-bacillithiolated under HOCl stress and *S*-itaconated by itaconic acid [34,35]. Interestingly, many targets for itaconation are redox-sensitive enzymes, which function in the regeneration of the thiol-redox homeostasis and ROS detoxification, including several thioredoxin (Trx)-like proteins (TrxA, TrxP, SACOL1794, NrdH), the thioredoxin reductase TrxB, the HOSCN reductase MerA, the peroxiredoxin AhpCF and the thiol peroxidase Tpx (Table 2, Table S8). These redox-sensitive enzymes were modified by itaconic acid at their conserved active site Cys residues, which are present in the CxxC motif in case of Trx family proteins. The antioxidant enzymes AhpCF and Tpx were previously identified as HOCl-sensitive in *S. aureus* and *E. coli* cells, showing significant basal oxidation [34,71]. Further targets for itaconation include metabolic enzymes (e.g. GuaB, PpaC, PdhC), translation elongation factors Tu and G (EF-Tu, EF-G) and ribosomal proteins

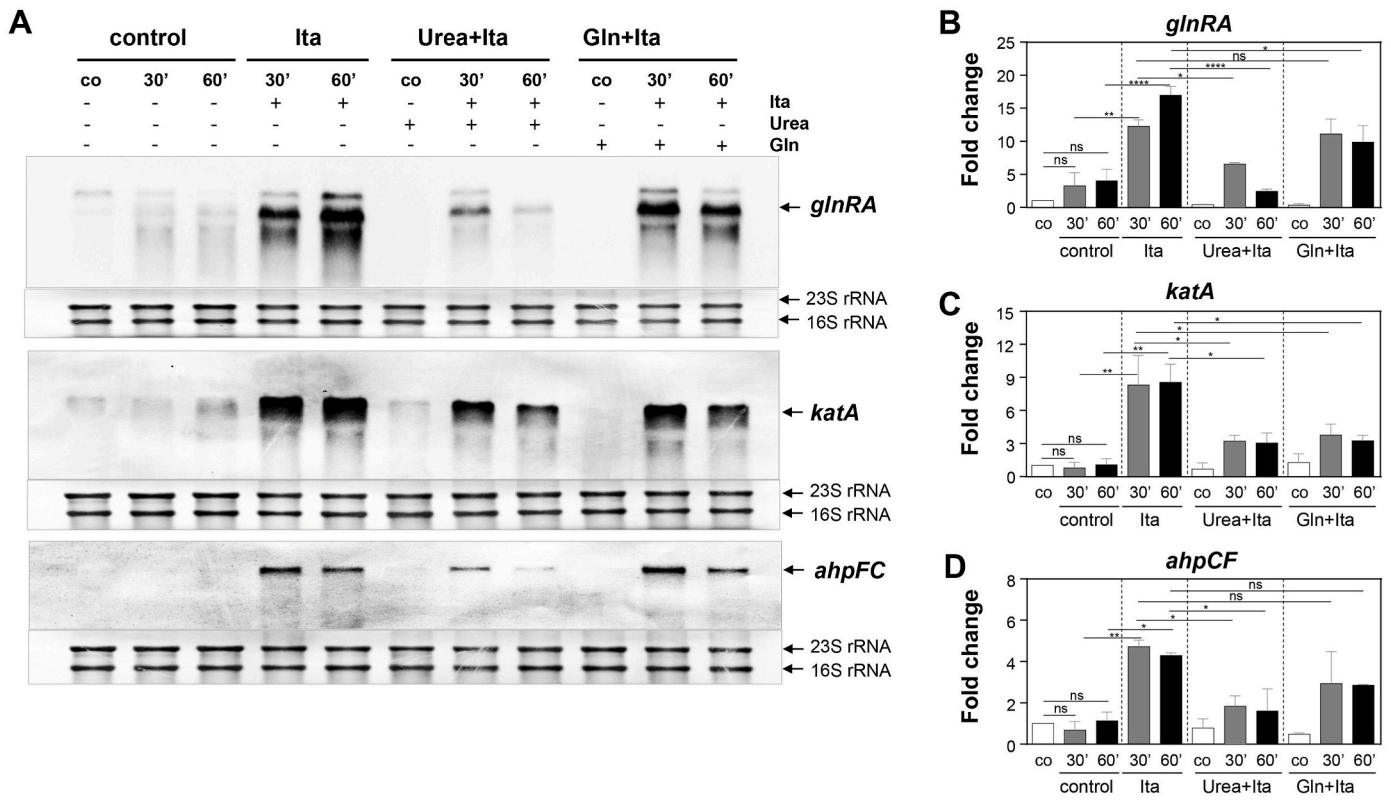

Fig. 7. Itaconic acid induces an acid-dependent ammonium limitation and ROS defense enzymes, as indicated by the GlnR and PerR regulons, which are affected by urea supplementation. *S. aureus* COL grown in RPMI with 20 mM urea or 20 mM glutamine until an OD_{500} of 0.5 was exposed to 13 mM itaconic acid. Northern blot analysis was used to analyze transcription of *glnRA*, *katA* and *ahpCF* in *S. aureus* COL after treatment with 13 mM itaconic acid for 30 and 60 min **(A)**. The methylene blue image below the Northern bots denotes the bands of the 16S and 23S rRNAs as RNA loading control. Quantification of the transcriptional induction of *glnRA* **(B)**, *katA* **(C)** and *ahpCF* **(D)** after itaconic acid stress in *S. aureus* was performed from the Northern blot images using ImageJ. Itaconic acid-induced fold-changes were calculated from 2 biological replicates and error bars represent the standard deviation (SD). The transcript levels were normalized to the mRNA level of the untreated control, which was set to 1. The statistics was calculated using a Student's unpaired two-tailed *t*-test by the graph prism software. Symbols are: $^{ns}p > 0.05$, $^{*}p \leq 0.05$, $^{**}p \leq 0.01$, $^{***}p \leq 0.001$ and $^{****}p \leq 0.0001$.

(RpmF, RpmJ, RpmG1, RpsR), which were modified at conserved Cys residues (Table 2, Table S8). Itaconation of RpmG1 and RpmJ occurred at their Zn-binding sites, which are sensitive to thiol-oxidation by HOCl stress [34]. Altogether, our results revealed that itaconic acid conjugates specifically active site Cys residues of Trx-like and antioxidant proteins, metabolic enzymes and ribosomal proteins, showing some overlap with the targets for HOCl-induced protein thiol-oxidation.

Antioxidants and acid stress resistance mechanisms function in the defense against itaconic acid. Next, we were interested to identify potential defense mechanisms against itaconic acid stress in *S. aureus*. The transcriptome analysis revealed that itaconic acid induces an acid and oxidative stress response (Fig. 2; Tables S3 and S4). Thus, we analyzed the growth and survival of the Δ*katA* and Δ*bshA* mutants, which are impaired in the oxidative stress defense (Fig. 9). In addition, the Δ*ccpA* and urease-deficient Δ*ureABCE* mutants were analyzed for growth and survival defects after itaconic acid stress, since the urease is known to provide protection against acid stress, which is controlled by the catabolite control protein A (CcpA) [61]. The Δ*katA*, Δ*bshA* and Δ*ureABCE* mutants did not show growth differences with itaconic acid as compared to the WT strain (Fig. 9A, B, D). However, the survival rates of the Δ*katA*, Δ*bshA* and Δ*ureABCE* mutants were strongly decreased after 2 and 4 h of itaconic acid stress, indicating that the catalase, BSH and the urease provide protection against itaconic acid in *S. aureus* (Fig. 9E and F). The sensitive phenotypes of the Δ*katA* and Δ*bshA* mutants could be restored back to WT levels in the *katA* and *bshA* complemented strains (Fig. 9E and F). However, due to the large deletion of the *ureABCE* gene cluster, plasmid-based complementation of the Δ*ureABCE* mutant was not possible. The Δ*ccpA* mutant was delayed in growth with or without itaconic acid in relation to the WT (Fig. 9C). In survival assays, the Δ*ccpA* mutant showed an itaconic acid resistance phenotype (Fig. 9E and F), which might be due to lower acetate secretion and higher ammonium generation as caused by increased amino acid catabolism, providing a growth advantage under weak acid stress as revealed previously [61,68]. Altogether, our phenotype results revealed that antioxidants (catalase, BSH), the urease and deletion of CcpA promote resistance towards itaconic acid stress in *S. aureus*.

4. Discussion

In this manuscript, we have used transcriptomic, redox proteomic and metabolomic analyses to study the antimicrobial mode of action of the immunometabolite itaconic acid and its effect on cellular metabolism in the pathogen *S. aureus*. Itaconate was previously shown to accumulate significantly in activated macrophages and neutrophils in response to *S. aureus* infections and promotes survival of neutrophils and the pathogen by reprogramming host-pathogen metabolism leading to biofilm formation [12,13,72]. Here we showed that sublethal concentrations of itaconic acid exert strong acid stress responses in *S. aureus* leading to a rapid acidic shift of the external pH, which was dependent on the starting pH of the bacterial culture. Due to the high starting pH of 8.5 in the RPMI-grown culture, the sublethal dose was determined as 13 mM itaconic acid, which resulted in a half-maximal growth and drop of the external pH to 5.5. The sublethal growth-inhibitory concentration of itaconic acid was decreased to 10 mM and 7 mM when the starting pH of the RPMI-grown culture was adjusted to pH 7.5 and 6.5, respectively, supporting previous data in *E. coli* and *S.* Typhimurium that the

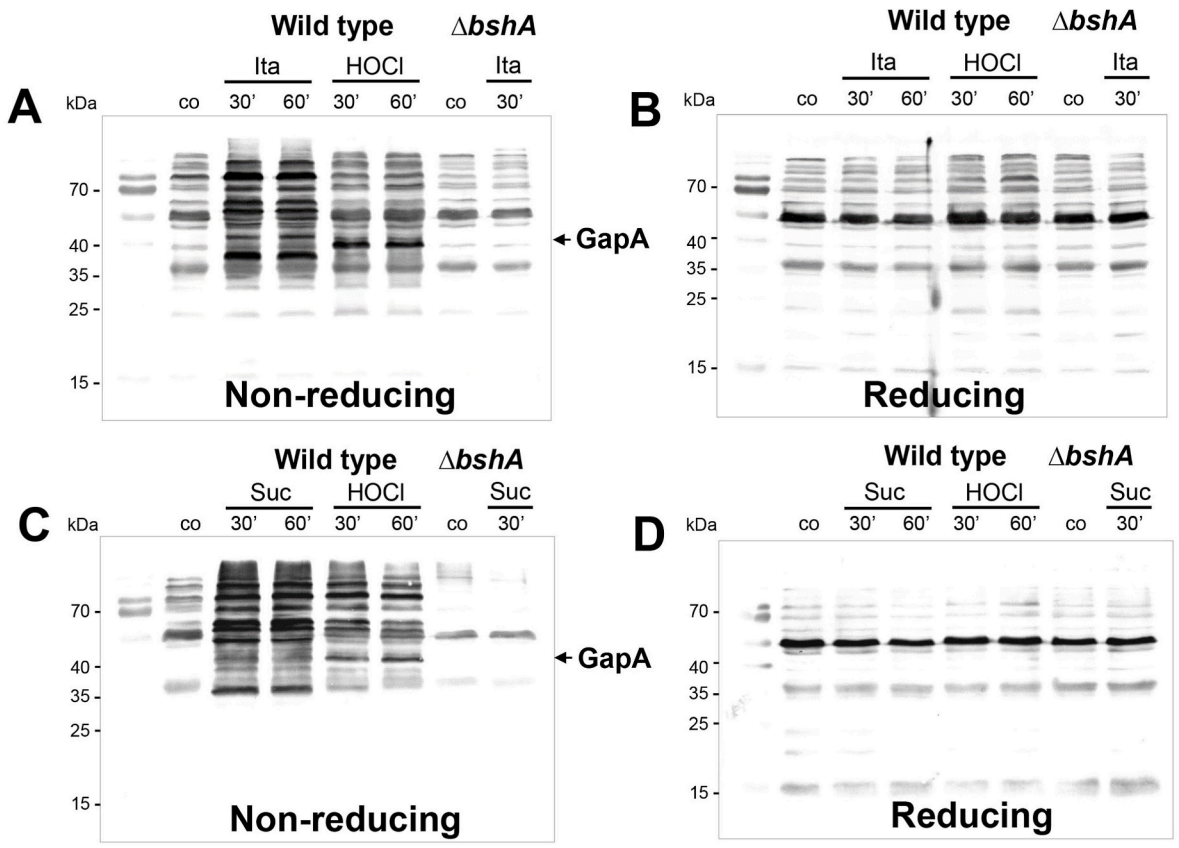

Fig. 8. Itaconic acid and succinic acid stress cause strong *S*-bacillithiolation in *S. aureus*. *S. aureus* COL wild type and the Δ*bshA* mutant were exposed to 13 mM itaconic acid **(A, B)** or 13 mM succinic acid **(C, D)** for 30 min. The NEM-alkylated protein extracts were subjected to BSH-specific non-reducing Western blot analysis. **(A, C)** Non-reducing BSH-specific Western blot analysis showed increasing levels of *S*-bacillithiolated proteins in *S. aureus* COL strain under itaconic acid and succinic acid stress. **(B, D)** Reducing BSH-specific Western blot are shown to validate the reversible *S*-bacillithiolations in A) and C). The corresponding protein loading controls are provided as SDS-PAGE images in Fig. S5.

increased acidity of the environment acts synergistic on the antimicrobial activity of itaconic acid as electrophile [24]. In contrast, stress exposure with the pH 7-adjusted itaconic acid resulted in the loss of the antimicrobial activity even at high concentrations of 50–70 mM (Fig. S6), which is consistent with previous reports [24]. This indicates that high acidity inside the phagolysosome potentiates the antimicrobial activity of physiological relevant concentrations of itaconic acid, which are in the range of 3–8 mM in murine macrophages [10,11], 60 μM in human macrophages [10] and 100–125 nM in the airway fluids after lung infection [13]. The concentration of itaconate was even determined as 5–6 mM inside the *Salmonella*-containing vacuole (SCV), where the intracellular pathogen *S.* Typhimurium replicates at pH 5 [73]. Thus, the growth-inhibitory concentrations applied in our studies are in the physiological range as encountered in the acidic phagosomes of macrophages at pH values of 4.5–5 after phagocytosis of pathogens [74]. In addition, itaconic acid might also synergize with other microbicidal oxidants, such as HOCl and HOSCN, which are secreted as part of the oxidative burst in the phagosome of neutrophils during infections [9,75]. To elucidate the synergy between the oxidants of the respiratory burst and itaconic acid in the acidic phagosome regarding the antimicrobial activity against pathogens is an interesting research question for future studies.

It is well known that *S. aureus* is very sensitive to weak organic acids, such as lactic and acetic acid, since these dissociate not completely into protons and anions, leading to the uptake of the membrane-permeable undissociated acid, which releases intracellular protons and acidifies the intracellular pH [56,76]. This proton shuttle effect was previously proposed as possible mode of action of itaconic acid, but detailed gene expression analysis of the specific stress responses was lacking, although the acidity of the environment is physiological relevant and an important contributor of the antimicrobial activity of itaconic acid [24]. The transcriptome signature supports the strong acid stress response and possible acidification of the cytoplasm upon itaconic acid stress as revealed by the induction of known acid stress mechanisms, including the urease-encoding *ureABCEFGD* operon and the *alsSD* operon, which function in neutralization by proton consumption and production of ammonium and the neutral acetoin instead of acetate (Fig. 10) [56]. The upregulation of the urease and the *alsSD* operon was reported in the transcriptome analysis by acetic acid as another weak organic acid [77]. The urease is a central player of the acid stress response network in *S. aureus*, which is essential for pH homeostasis and virulence and contributes to acid stress resistance [56,59,61,78].

Our transcriptome results further identified the K^+ ATPase-encoding *kdpABCF* operon as most highly upregulated under itaconic acid stress, supporting that the uptake of K^+ ions contributes to pH homeostasis to maintain the internal neutral pH under acid stress (Fig. 10). The involvement of K^+ uptake in pH homeostasis and the proton motive force (PMF) under acid stress has been revealed in many bacteria, including *Lactococcus lactis, E. coli, Enterococcus faecalis, Streptococcus mutans*, *Corynebacterium glutamicum* and *S. aureus* [79–86]. The PMF consists of the chemical pH gradient ΔpH and an electric gradient ΔΨ, which are related by the following equation $PMF = \Delta\Psi - Z\,\Delta pH$ ($Z = 2.3\,RT/F$) [84]. As shown in *E. coli* and *C. glutamicum*, a sudden pH decrease leads to an increased ΔpH and consequently an increased electrochemical proton potential, the PMF as driving force for the influx of protons via the ATP synthase, resulting in a decrease of the internal pH [80,84]. Since maintenance of a neutral internal pH is crucial for survival under acid stress, the bacteria counteract this internal pH decrease

Table 1
Identifications of *S*-bacillithiolations in the proteome of *S. aureus* COL after exposure to 13 mM itaconic acid.

Accession	Gene	Locus tag	Protein function	pep_exp_mz	pep_exp_mr	pep_exp_z	pep_calc_mr	pep_delta	pep_score	pep_expect	pep_seq	Cys + BSH
A0A0H2WWJ4	trxA3	SACOL1992	Thioredoxin family protein	886.4113	2656.212	3	2656.2144	−0.0024	69.05	1.20E-07	VLVITEDWC$_{63}$GDAMMNLPILK	Cys63*+BSH
A0A0H2WZ97	brxC	SACOL0804	Monothiol bacilliredoxin BrxC	774.3145	2319.9217	3	2319.926	−0.0043	27.30	0.0019	HSETC$_{30}$PISANAYDQFNK	Cys30*+BSH
Q5HIC4	hchA	SACOL0597	Glyoxalase-III/chaperone HchA	1165.1906	3492.55	3	3492.5589	−0.0089	96.30	2.30E-10	SPLEGYSVC$_{214}$VFPDSLDEGANIEIGYLPGR	Cys214*+BSH
Q5HIC7	tuf	SACOL0594	Elongation factor Tu	703.2861	2106.8364	3	2106.8411	−0.0048	28.05	0.0016	HYAHVDC$_{82}$PGHADYVK	Cys82*+BSH
Q5HIQ7	guaB	SACOL0460	Inosine-5∼-monophosphate dehydrogenase	843.7313	2528.1721	3	2528.1775	−0.0053	31.65	0.00068	VVAGVGVPQITAIYDC$_{326}$ATEAR	Cys326+BSH
Q5HHP5	gapA	SACOL0838	Glyceraldehyde-3-phosphate dehydrogenase	947.4371	3785.7195	4	3785.7248	−0.0053	30.06	0.00099	TIVFNTNHQELDGSETVVSGASC$_{151}$TTNSLAPVAK	Cys151*+BSH
A0A0H2WZN5	tal	SACOL1831	Transaldolase	990.468	2968.3823	3	2968.3933	−0.011	34.01	0.0004	ELFNVIQADEIGADIITC$_{198}$PADVVK	Cys198+BSH
Q5HHP3	tpiA	SACOL0840	Triosephosphate isomerase	856.4178	2566.2316	3	2566.2394	−0.0077	54.47	3.60E-06	EVESVIC$_{40}$APAIQLDALTTAVK	Cys40+BSH
Q5HI88	pta	SACOL0643	Phosphate acetyltransferase	1193.5271	3577.5595	3	3577.56	−0.0005	104.7	3.40E-11	GDEQYIFGDC$_{78}$AINPELDSQGLAEIAVESAK	Cys78+BSH
Q5HGY9	pdhC	SACOL1104	Dihydrolipoyllysine-residue acetyltransferase	933.9522	3731.7799	4	3731.7924	−0.0125	28.17	0.0018	GATC$_{346}$TISNIGSAGGQWFTPVINHPEVAILGIGR	Cys346+BSH
Q5HGY8	pdhD	SACOL1105	Dihydrolipoyl dehydrogenase	1103.5006	4409.9733	4	4409.9753	−0.002	56.74	2.10E-06	VAAEAIDGQAAEVDYIGMPAVC$_{352}$FTEPELATVGYSEAQAK	Cys352+BSH
Q5HCU5	mqo2	SACOL2623	Malate:quinone oxidoreductase 2	801.6229	3202.4624	4	3202.47	−0.0075	42.47	5.70E-05	HLGGFPISGQFLAC$_{275}$TNPQVIEQHDAK	Cys275*+BSH
Q5HGC3	glnA	SACOL1329	Glutamine synthetase	685.9539	2054.8399	3	2054.8449	−0.005	37.22	0.00019	YADAVTAC$_{210}$DNIQTFK	Cys210+BSH
Q5HGC3	glnA	SACOL1329	Glutamine synthetase	636.9506	1907.8301	3	1907.8281	0.002	14.19	0.038	GFTAVC$_{291}$NPLVNSYK	Cys291+BSH
Q5HHC7	gluD	SACOL0961	NAD-specific glutamate dehydrogenase	881.4067	3521.5978	4	3521.6065	−0.0087	27.58	0.0017	ELFELDC$_{286}$DILVPAAISNQITEDNAHDIK	Cys286+BSH
Q5HIS8	ssb	SACOL0438	Single-stranded DNA-binding protein 1	779.0268	2334.0587	3	2334.0647	−0.0061	29.78	0.0011	VFVTEVVC$_{97}$DSVQFLEPK	Cys97+BSH

S. aureus COL was exposed to 13 mM itaconic acid for 30 min and the proteome samples were prepared as described in the Methods section. The *S*-bacillithiolated Cys peptides were identified using Orbitrap Q Exactive shotgun LC-MS/MS analysis based on the mass shift of 396 Da for bacillithiol ($C_{13}H_{20}N_2O_{10}S_1$) at Cys peptides. The BSH-modified peptides were further validated by the characteristic malate neutral loss ions (Cys+134.021523 for $C_4H_6O_5$), which was included in the Mascot search. The table lists the Uniprot-accession number, gene name, protein function and the quality control criteria for the *S*-bacillithiolated Cys peptides as obtained from the LC-MS/MS analysis and the Mascot search results, including the measured peptide *m/z* value, experimental mass, charge state, calculated (theoretical) mass, mass deviation (in Da), Mascot score and Mascot expect value. The modified active site Cys residues are marked with *. For each *S*-bacillithiolated Cys peptide only one representative peptide is shown in the table while the complete Mascot search results and *S*-bacillithiolated peptides identified in 3 replicates, including the MS/MS spectra and fragment ion tables are shown in Table S7.

Table 2
Identification of Cys-itaconation in the proteome of *S. aureus* COL after exposure to 13 mM itaconic acid.

Accession	Gene	Locus tag	Protein function	pep_exp_mz	pep_exp_mr	pep_exp_z	pep_calc_mr	pep_delta	pep_score	pep_expect	pep_seq	Cys + Itaconate
Q5HIR5	ahpC	SACOL0452	Alkyl hydroperoxide reductase C	624.9636	1871.8691	3	1871.8723	−0.0032	44.08	3.90E-05	KNPGEVC$_{168}$PAKWEEGAK	Cys168+C5H6O4
Q5HIR6	ahpF	SACOL0451	Alkyl hydroperoxide reductase subunit F	663.6205	1987.8397	3	1987.8445	−0.0048	44.3	3.70E-05	GVAFC$_{335}$PHCDGPLFENK	Cys335+C5H6O4
Q5HF61	tpx	SACOL1762	Thiol peroxidase	1031.0112	2060.0078	2	2060.0096	−0.0018	95.47	2.80E-10	LISVVPSIDTGVC$_{60}$DQQTR	Cys60*+C5H6O4
Q5HGT9	trxA	SACOL1155	Thioredoxin	1190.537	2379.0594	2	2379.0552	0.0043	99.21	1.20E-10	VESGVQLVDFWATWC$_{29}$GPCK	Cys29*+C5H6O4
SACOL0829	trxB	SACOL0829	Thioredoxin reductase	861.3609	1720.7072	2	1720.7113	−0.0041	36.03	0.00025	GVSYC$_{134}$AVCDGAFFK	Cys134*+C5H6O4
A0A0H2WVJ7	trxP	SACOL0875	Thioredoxin, reduces persulfides	719.7714	1437.5283	2	1437.5329	−0.0046	45.11	3.10E-05	FEAGWC$_{29}$PDCR	Cys29*+C5H6O4
A0A0H2WZ00	trxA2	SACOL1794	Thioredoxin, putative	1071.9466	2141.8786	2	2141.8823	−0.0037	92.84	5.20E-10	QGATVFEFTAGWC$_{27}$PDCR	Cys27*+C5H6O4
A0A0H2WYJ6	nrdH	SACOL1093	Redoxin of ribonucleotide reductase	1156.5251	2311.0356	2	2311.0388	−0.0032	33.98	0.0004	SEIIVYTQNDC$_{12}$PPCTFVK	Cys12*+C5H6O4
SACOL0640	merA	SACOL0640	Pyridine nucleotide-disulfide oxidoreductase	906.403	1810.7915	2	1810.794	−0.0025	44.73	3.40E-05	MYGGTC$_{43}$INIGCIPSK	Cys43*+C5H6O4
Q5HIC8	fusA	SACOL0593	Elongation factor G	972.9255	1943.8364	2	1943.8393	−0.0029	45.49	2.80E-05	EFNVEC$_{473}$NVGAPMVSYR	Cys473+C5H6O4
Q5HIC7	tuf	SACOL0594	Elongation factor Tu	921.3962	1840.7779	2	1840.7839	−0.006	57.66	1.70E-06	HYAHVDC$_{82}$PGHADYVK	Cys82*+C5H6O4
Q5HGV6	rpmF	SACOL1137	50S ribosomal protein L32	991.911	1981.8073	2	1981.8107	−0.0034	55.28	3.00E-06	ISVPGMTEC$_{30}$PNCGEYK	Cys30*+C5H6O4
Q5HFK9	rpmG1	SACOL1608	50S ribosomal protein L33	818.351	1634.6875	2	1634.6916	−0.0041	89.76	1.10E-09	VNVTLAC$_{9}$TECGDR	Cys9+C5H6O4
Q5HDY1	rpmJ	SACOL2216	50S ribosomal protein L36	693.374	1384.7335	2	1384.7384	−0.0049	35.41	0.00033	VRPSVKPIC$_{11}$EK	Cys11*+C5H6O4
Q5HIS7	rpsR	SACOL0439	30S ribosomal protein S18	625.6236	1873.849	3	1873.8557	−0.0066	49.42	1.10E-05	VC$_{16}$YFTANGITHIDYK	Cys16*+C5H6O4
A0A0H2WXG3	SACOL2532	SACOL2532	Acetyltransferase, GNAT family	535.264	1068.5135	2	1068.5161	−0.0026	32.26	0.00059	IIASC$_{75}$SFAK	Cys75*+C5H6O4
Q5HDX9	adk	SACOL2218	Adenylate kinase	732.3405	2193.9997	3	2194.0187	−0.019	48.63	1.40E-05	RICESC$_{130}$GTTYHLVFNPPK	Cys130+C5H6O4
Q5HFJ5	glyQS	SACOL1622	Glycine–tRNA ligase	759.3744	1516.7342	2	1516.7331	0.0012	43.63	6.50E-05	IIDDEGIVC$_{137}$PVSK	Cys137+C5H6O4
Q5HIQ7	guaB	SACOL0460	Inosine-5~-monophosphate dehydrogenase	645.8169	1289.6192	2	1289.6286	−0.0093	45.26	3.00E-05	VGIGPGSIC$_{307}$TTR	Cys307*+C5H6O4
Q5HGY8	pdhD	SACOL1105	Dihydrolipoyl dehydrogenase	893.4266	1784.8386	2	1784.8437	−0.0051	100.11	1.30E-10	GNLGGVC$_{47}$LNVGCIPSK	Cys47*+C5H6O4
Q5HEK1	ppaC	SACOL1982	Manganese-dependent inorganic pyrophosphatase	792.8682	1583.7219	2	1583.729	−0.007	60	1.00E-06	IANFETAGPLC$_{118}$YR	Cys118*+C5H6O4
Q5HGK3	fabD	SACOL1244	Malonyl CoA-acyl carrier protein transacylase	713.6052	2850.3918	4	2850.4069	−0.0151	29.65	0.0011	SLSSDDKIIEPANINC$_{161}$PGQIVVSGHK	Cys161+C5H6O4
Q5HDR3	sarR	SACOL2287	HTH-type transcriptional regulator SarR	754.8513	1507.6881	2	1507.6905	−0.0024	27.26	0.0019	C$_{57}$SEFKPYYLTK	Cys57+C5H6O4

S. aureus COL was exposed to 13 mM itaconic acid for 30 min and the proteome samples were prepared as described in the Methods section. The itaconated Cys peptides were identified using Orbitrap Q Exactive shotgun LC-MS/MS analysis according to a mass increase of 130 Da for $C_5H_6O_4$ at Cys peptides. The table lists the Uniprot-accession number, gene name, protein function and the quality control criteria for the itaconated Cys peptides as obtained from the LC-MS/MS analysis and the Mascot search results, including the measured peptide *m/z* value, experimental mass, charge state, calculated (theoretical) mass, mass deviation (in Da), Mascot score and Mascot expect value. The modified active site Cys residues are marked with *. For each itaconated Cys peptide only one representative peptide is shown in the table while the complete Mascot search results and itaconated Cys peptides identified in 3 replicates, including the MS/MS spectra and fragment ion tables are shown in Table S8.

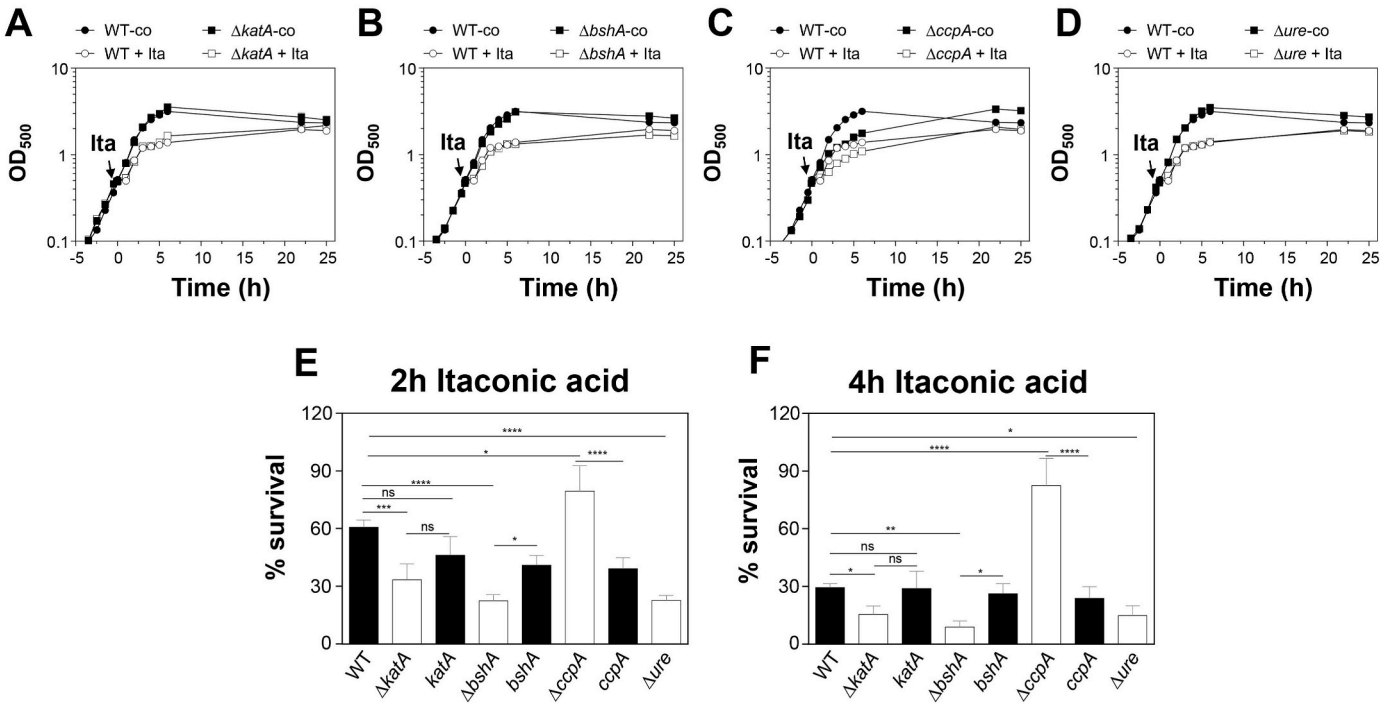

Fig. 9. Deletion of *katA, bshA* and *ureABCE* leads to increased itaconic acid sensitivity while loss of *ccpA* promotes survival of *S. aureus* under itaconic acid stress. The *S. aureus* COL WT, Δ*katA,* Δ*bshA*, Δ*ureABCE* and Δ*ccpA* mutants were grown in RPMI until an OD_{500} of 0.5 and treated with 13 mM itaconic acid to monitor the growth curves **(A–D)**. The survival rates of the CFUs for the itaconic acid-treated samples were calculated from WT, Δ*katA,* Δ*bshA*, Δ*ureABCE* and Δ*ccpA* mutants and the complemented strains at 2 h **(E)** and 4 h **(F)** after stress exposure relative to the control, which was set to 100%. Mean values of four biological replicates are presented. Error bars represent the standard deviation. The statistics was calculated using a Student's unpaired two-tailed *t*-test by the graph prism software. Symbols are: $^{ns}p > 0.05$, $^{*}p \leq 0.05$, $^{**}p \leq 0.01$, $^{***}p \leq 0.001$ and $^{****}p \leq 0.0001$.

by lowering the membrane potential (ΔΨ) through the uptake of positively charged K^+ ions by various high affinity potassium transporters [80,84]. In *S. aureus* potassium uptake is mediated by the medium affinity Ktr transporter under neutral and alkaline conditions, while the high affinity KdpABCF ATPase is induced and required for K^+ uptake under acid stress due to K^+ limitation [85,87]. Thus, itaconic acid leads to K^+ uptake by the KdpABCF transporter to decrease ΔΨ to maintain a constant electrochemical proton potential (PMF) and pH homeostasis in *S. aureus.* In the metabolome, itaconic acid caused a strongly enhanced intracellular level of lysine, whose accumulation depends on the membrane potential in exchange of potassium [69]. Thus, the ammonium group of the side chain of lysine could contribute to pH neutralization upon itaconic acid stress. The strong downregulation of the ATP synthase-encoding *atp* operon under itaconic acid stress and other acid stress conditions [56] might prevent the influx of protons under acid shock conditions.

Furthermore, K^+ limitation affects the energy metabolism of *S. aureus* by shifting the carbon flux from oxidative phosphorylation toward substrate-level phosphorylation by enhanced glycolysis and overflow metabolism while the electron transport chain activity is decreased [86]. Our data showed the upregulation of the glycolytic pathway in the transcriptome and increased pyruvate and acetoin secretion via AlsSD upon itaconic acid stress, while the *atp* operon for ATP synthesis and the terminal oxidase-encoding *qoxABCD* and *cydAB* operons were repressed. However, external glucose and internal glycolytic and TCA cycle metabolites declined within 120 min after t0 with no significant differences between control and itaconic acid-treated cells, making it difficult to conclude about the glycolytic activity after itaconic acid stress. A previous study revealed that growth of *S. aureus* LAC in pH-neutralized LB medium with 30 mM itaconate results in decreased glycolysis due to itaconation and inhibition of the fructose-1, 6-bisphosphate aldolase Fba, leading to redirection of the carbon flow to UDP-*N*-acetyl-glucosamine synthesis for polysaccharide intracellular adhesion (PIA)-dependent biofilm formation [12]. In our work, transcription of the *icaADBC* operon for biofilm formation was decreased upon itaconic acid stress in *S. aureus*. The differences in metabolic regulation in these two studies might due to the strains (COL vs. LAC) or the stress experiments (addition of sublethal itaconic acid to exponentially growing cells in RPMI vs. growth in pH-controlled itaconate-supplemented LB medium) as biofilm-formation requires specific growth conditions and isolate-dependent differences were previously reported [88,89].

However, our metabolomics data showed that itaconic acid strongly impacts the uptake and metabolism of several amino acids, leading to intracellular accumulation of lysine, threonine, aspartate, alanine, valine, leucine, isoleucine, histidine, methionine and cysteine. Similarly, the uptake of amino acids was affected during different growth phases and environmental stress conditions, such as osmotic, heat and pH stress [90]. The reasons for the increased intracellular levels of the amino acids are unknown, since transcription of known amino acid or peptide transporters and amino acid biosynthesis pathways (e.g. for lysine, cysteine) was not upregulated in the transcriptome analysis. Although *S. aureus* can synthesize many amino acids, the uptake from the medium is always preferred over new synthesis [90]. However, the substrates and functions of the majority of >100 putative amino acid, peptide or osmolyte membrane transporters, which are annotated in the *S. aureus* genomes remain to be elucidated [91]. As amino acid transporters have been associated with virulence and antibiotics resistance, these might be not only involved in the differential amino acid uptake upon stress and starvation, but also important targets for therapeutic interventions [91].

The potassium uptake occurs as initial response towards hyperosmotic stress, followed by synthesis or uptake of compatible solutes, such as glycine-betaine or proline [92]. Both the *kdpABCF* and *opuCA-CB-CC-CD* operons for the uptake of potassium and glycine betaine, respectively, are upregulated under itaconic acid and mild acid stress of pH 5.5 [59], suggesting a protective role of compatible solutes under

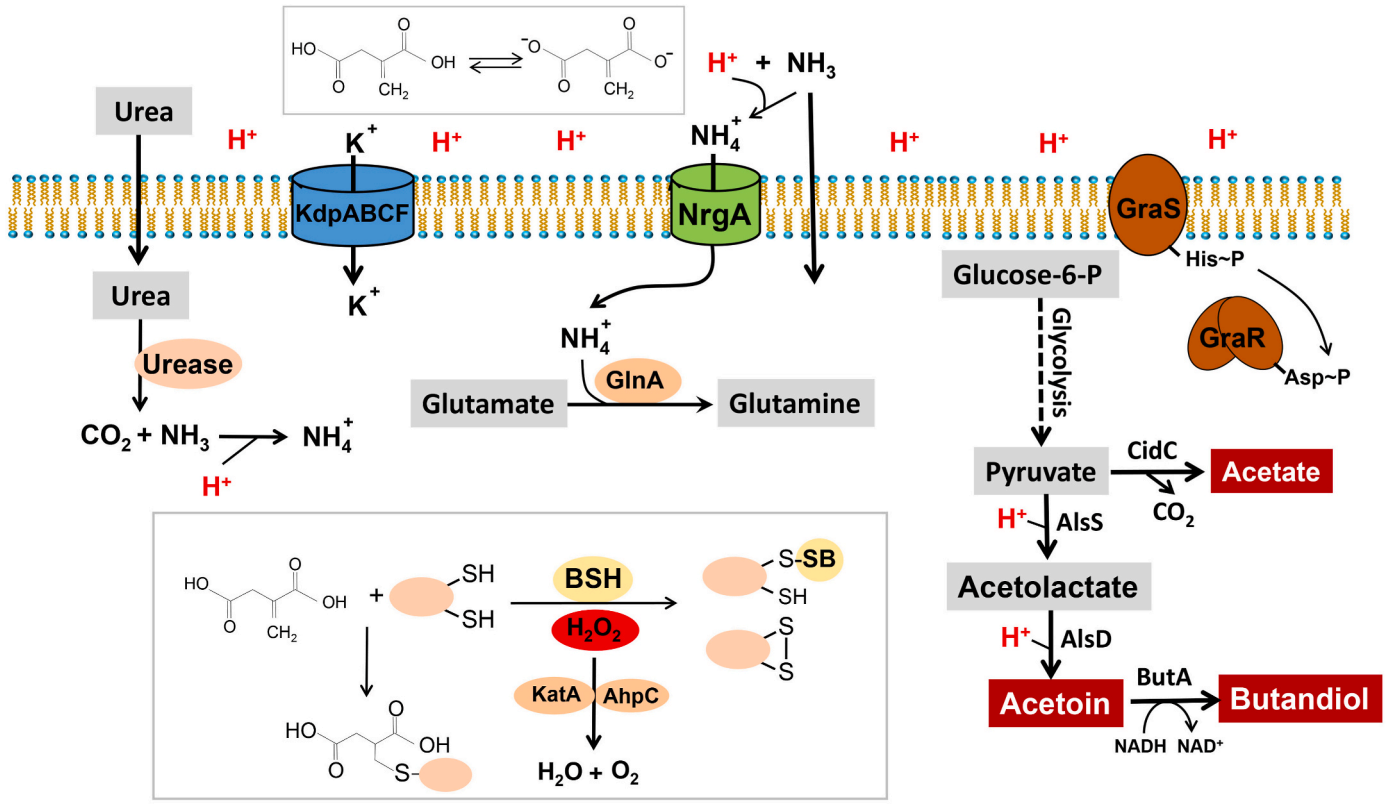

Fig. 10. Summary of the main mode of action of itaconic acid in *S. aureus*. Itaconic acid is a weak dicarboxylic acid, which induces acid stress and ammonium limitation since protonated ammonium cannot freely diffuse the cytoplasmic membrane and requires the high affinity transporter NrgA for uptake. Ammonium limitation leads to induction of the GlnR regulon, including the glutamine synthetase GlnA and the transporter NrgA. *S. aureus* cells neutralize the acid stress by increased urease expression, which generates ammonium from urea. In addition, potassium uptake via the KdpABCF potassium transporting ATPase is induced as counter ion for protons to balance pH homeostasis and the PMF. Induction of the GraRS regulon indicates cell wall stress due to acidification. The AlsSD α-acetolactate synthase/decarboxylase pathway is induced, which consumes protons to produce the neutral product acetoin from pyruvate to restore pH homeostasis. *S. aureus* further encounters oxidative and electrophile stress, since increased protein *S*-bacillithiolation and *S*-itaconation of redox-sensitive enzymes were observed in the proteome of itaconic acid-treated cells. Phenotype analyses further revealed that the catalase KatA, BSH and the urease protect against acid and oxidative stress provoked by itaconic acid.

acid stress. Recent studies have established that the second messenger cyclic di-adenosine monophosphate (c-di-AMP) plays a central role in regulation of potassium homeostasis and osmoprotection in many firmicutes, including *B. subtilis* and *S. aureus* [93,94]. Among the targets inhibited under potassium excess by high c-di-AMP levels are the KdpD sensor kinase of the high affinity KdpABCE transporter and the ATPase subunit OpuCA to prevent toxic accumulation of potassium and osmolytes in the cells [94,95]. Under K^+ limitation, the level of c-di-AMP is low, leading to upregulation of high affinity transporters for K^+ and compatible solutes to restore osmotic and potassium homeostasis [93]. Thus, the exposure to itaconic acid most likely decreases the c-di-AMP levels to upregulate the uptake of K^+ and compatible solutes in *S. aureus* for pH homeostasis and protection against acid-induced protein damage, which remains to be further explored.

In addition, the major response to itaconic acid was revealed as the strong induction of the GlnR regulon, including the ATP-dependent glutamine synthetase GlnA and the high affinity ammonium transporter NrgA, which respond to ammonium limitation under acid stress (Fig. 10) [60,96]. GlnA has a high affinity for ammonium, which is incorporated into glutamate to generate glutamine under nitrogen limitation. The uptake of ammonium depends on the external pH, since only uncharged ammonia can freely diffuse the membrane, while the protonated charged ammonium is present at acidic external pH, which cannot diffuse and requires the high affinity ammonium transporter NrgA (AmtB) [60,96]. Thus, the *glnRA* operon and *nrgA* are upregulated upon itaconic acid stress due to ammonium limitation, to facilitate ammonium uptake for glutamine synthesis and neutralization of the external pH. Using supplementation experiments with either an excess of 20 mM glutamine or 20 mM urea, which is converted to ammonium by the urease [61], we could confirm that the *glnRA* operon responds to ammonium limitation due to the low pH. The external pH was increased by urea and the expression of the *glnRA* operon was subsequently decreased, while an excess of glutamine could not neutralize the pH and expression of the *glnRA* operon remained high. Thus, the low external pH caused by itaconic acids leads to ammonium starvation, which can be abolished by urea supply due to the urease function. Consistent with the pH neutralization upon urea supply, the growth of the itaconic acid- and succinic acid-treated cultures was strongly improved. Phenotype analysis further showed that the urease-deficient Δ*ureABCE* mutant was highly sensitive to itaconic acid, indicating that the urease provides resistance against itaconic acid. Our results are thus consistent with previous studies, showing that the urease is a central component of pH homeostasis under weak acid stress in urea-rich environments [61]. *S. aureus* can cause infections in urea-rich niches of the human body, such as the human sweat of the skin, the saliva, the kidney and the urinary tract [97–100]. Accordingly, the urease was shown to promote survival during persistent and chronic kidney infections [61]. In addition, *S. aureus* ST1 strains were isolated from patients with clinical urinary tract infections (UTIs), which overproduced the urease constitutively showing persistence in a mouse model of UTI [101]. Thus, itaconic acid might be less effective as antimicrobial against *S. aureus* infections in urea-rich niches, which remains to be investigated using different infection models.

Acid stress has been previously associated with increased ROS

formation in *S. aureus* due to upregulation of genes with ROS detoxification functions, such as superoxide dismutases (*sodA*, *sodM*), the catalase (*katA*) and the peroxiredoxin (*ahpCF*) [56]. In addition, SodA was shown to confer resistance against ROS generated during acid stress [102]. In this work, we showed that itaconic acid led to strong induction of the peroxide-responsive PerR regulon, including *katA, ahpCF* and genes involved in iron storage (*dps, ftnA*) [30]. The *katA* mutant was sensitive in survival under itaconic acid stress, supporting that KatA is involved in detoxification of H_2O_2 produced during itaconic acid treatment. KatA was shown to remove the majority of H_2O_2 providing resistance towards high levels of 100 mM H_2O_2 in aerobic cells [49,103]. However, the itaconic acid-induced transcription of *katA* and *ahpCF* was only partially abolished upon neutralization of the external pH with urea, supporting that itaconic acid exerts its action as electrophile independently of the acid stress mode of action. Furthermore, the addition of the antioxidant N-acetyl cysteine as ROS quencher did not improve the growth of the itaconic acid-treated culture, indicating that the acidification was the main determinant of the antimicrobial mode of action as supported also by the growth experiments with urea.

To further understand the oxidative and electrophile mode of action, we studied the post-translational thiol-modification caused by itaconic acid in the proteome of *S. aureus*. Due to the strong induction of the oxidative stress-specific PerR regulon, we were interested to analyze reversible protein *S*-bacillithiolations, which were previously caused by strong oxidants encountered during infections, such as HOCl stress in *S. aureus* [34,35]. Thus, reversible S-bacillithiolations serve as an indicator of the oxidative mode of action, while *S*-itaconations are provoked by the alkylation chemistry as electrophilic mode of action of itaconic acid. Using BSH-specific non-reducing Western blot analysis and shotgun LC-MS/MS analyses, we identified significantly increased *S*-bacillithiolations and *S*-itaconations in the proteome of *S. aureus* cells, indicating that itaconic acid causes oxidative and electrophile stress. In survival assays, the *bshA* mutant was more susceptible towards itaconic acid than the WT, pointing to an important role of BSH as LMW thiol to protect proteins by *S*-bacillithiolation. The comparison of the proteins identified with *S*-bacillithiolation and *S*-itaconation sites revealed only a limited overlap. Several *S*-bacillithiolated proteins are involved in energy metabolism and biosynthesis pathways, including GapA, GuaB, Tal, TpiA, Pta, PdhC, PdhD, Mqo2, GlnA and GluD, which are abundant in the proteome according to previous studies [34]. While GapA and GuaB were previously shown to be *S*-bacillithiolated under HOCl stress at their active site Cys residues [34], which are involved in catalysis, the majority of other metabolic enzymes are not oxidized at conserved or active site Cys residues.

In contrast, out of the 23 identified *S*-itaconated proteins, 9 proteins are redox-sensitive Trx-like proteins (TrxA, TrxA2, TrxB, TrxP), peroxiredoxins (Tpx, AhpCF) and other thiol-disulfide oxidoreductases (NrdH, MerA), involved in detoxification of oxidants and regeneration of the redox homeostasis, which are *S*-itaconated at their redox-active centers, such as CxxC motifs in Trx-like proteins. Thus, itaconation targets not only abundant proteins, such as ribosomal proteins and translation factors, but also low abundant redox enzymes with reactive Cys residues. Moreover, the ribosomal proteins RpmJ and RpmG3 were *S*-itaconated within their Zn^{2+} redox switch motifs, which displayed increased thiol-oxidation under HOCl stress using the OxICAT approach [34]. Ribosomal proteins with Zn^{2+} redox switch motifs were proposed to serve as reservoir for Zn^{2+} storage, since they are not essential and have non-Zn^{2+} paralogs [104]. Upon Zn^{2+} limitation, the ribosomal Zn containing proteins RpmJ and RpmE were shown to be released from the ribosome and replaced by their paralogs YkgO and YkgM, which interact with the ribosome [105]. Overall, 4 ribosomal proteins (RpmJ, RpmG1, RpmF and RpsR) and the translation elongation factors EF-Tu and EF-Ts were *S*-itaconated, which might affect protein translation under itaconic acid stress. In addition, itaconation is an irreversible Cys-alkylation mechanism and the question arises how the cells can recover from itaconic acid stress, whether there are mechanisms mediating the reversibility of the modification. However, our shotgun approach does not provide information on the quantitative percentage of itaconation for each protein. Thus, future attempts are directed to develop enrichment tools and quantitative proteomics methods to analyze the fraction of itaconation in the proteome and the mechanisms of the recovery from itaconic acid stress in *S. aureus*.

Author disclosure statement

No competing financial interests exist.

Declaration of competing interest

No competing financial interests exist.

Acknowledgements

This work was supported by grants from the Deutsche Forschungsgemeinschaft DFG), Germany (AN746/4-1 and AN746/4-2) within the SPP1710 on “Thiol-based Redox switches”, by the SFB973 (project C08) and TR84 (project B06) to H.A. Metabolomics analysis is supported by the DFG grant LA1289/9-1 within the SPP 2389 on ”Emergent Functions of Bacterial Multicellularity” (project number 503880638) to M.L. For Orbitrap Q Exactive mass spectrometry by B.K., we would like to acknowledge the assistance of the Core Facility BioSupraMol supported by the DFG.

Appendix A. Supplementary data

Supplementary data to this article can be found online at https://doi.org/10.1016/j.freeradbiomed.2023.09.031.

References

[1] T.J. Foster, The *Staphylococcus aureus* "superbug", J. Clin. Invest. 114 (12) (2004) 1693–1696.
[2] F.D. Lowy, *Staphylococcus aureus* infections, N. Engl. J. Med. 339 (8) (1998) 520–532.
[3] H.W. Boucher, G.R. Corey, Epidemiology of methicillin-resistant *Staphylococcus aureus*, Clin. Infect. Dis. 46 (Suppl 5) (2008) S344–S349.
[4] G.L. Archer, *Staphylococcus aureus*: a well-armed pathogen, Clin. Infect. Dis. 26 (5) (1998) 1179–1181.
[5] H.F. Chambers, F.R. Deleo, Waves of resistance: *Staphylococcus aureus* in the antibiotic era, Nat. Rev. Microbiol. 7 (9) (2009) 629–641.
[6] M. Vestergaard, D. Frees, H. Ingmer, Antibiotic resistance and the MRSA problem, Microbiol. Spectr. 7 (2) (2019).
[7] A. Ulfig, L.I. Leichert, The effects of neutrophil-generated hypochlorous acid and other hypohalous acids on host and pathogens, Cell. Mol. Life Sci. 78 (2) (2021) 385–414.
[8] C.C. Winterbourn, A.J. Kettle, Redox reactions and microbial killing in the neutrophil phagosome, Antioxidants Redox Signal. 18 (6) (2013) 642–660.
[9] C.C. Winterbourn, A.J. Kettle, M.B. Hampton, Reactive oxygen species and neutrophil function, Annu. Rev. Biochem. 85 (2016) 765–792.
[10] A. Michelucci, T. Cordes, J. Ghelfi, A. Pailot, N. Reiling, O. Goldmann, T. Binz, A. Wegner, A. Tallam, A. Rausell, M. Buttini, C.L. Linster, E. Medina, R. Balling, K. Hiller, Immune-responsive gene 1 protein links metabolism to immunity by catalyzing itaconic acid production, Proc. Natl. Acad. Sci. U. S. A. 110 (19) (2013) 7820–7825.
[11] C.L. Strelko, W. Lu, F.J. Dufort, T.N. Seyfried, T.C. Chiles, J.D. Rabinowitz, M. F. Roberts, Itaconic acid is a mammalian metabolite induced during macrophage activation, J. Am. Chem. Soc. 133 (41) (2011) 16386–16389.
[12] K.L. Tomlinson, T.W.F. Lung, F. Dach, M.K. Annavajhala, S.J. Gabryszewski, R. A. Groves, M. Drikic, N.J. Francoeur, S.H. Sridhar, M.L. Smith, S. Khanal, C. J. Britto, R. Sebra, I. Lewis, A.C. Uhlemann, B.C. Kahl, A.S. Prince, S.A. Riquelme, *Staphylococcus aureus* induces an itaconate-dominated immunometabolic response that drives biofilm formation, Nat. Commun. 12 (1) (2021) 1399.
[13] K.L. Tomlinson, S.A. Riquelme, S.U. Baskota, M. Drikic, I.R. Monk, T.P. Stinear, I. A. Lewis, A.S. Prince, *Staphylococcus aureus* stimulates neutrophil itaconate production that suppresses the oxidative burst, Cell Rep. 42 (2) (2023), 112064.
[14] M. Bambouskova, L. Gorvel, V. Lampropoulou, A. Sergushichev, E. Loginicheva, K. Johnson, D. Korenfeld, M.E. Mathyer, H. Kim, L.H. Huang, D. Duncan, H. Bregman, A. Keskin, A. Santeford, R.S. Apte, R. Sehgal, B. Johnson, G. K. Amarasinghe, M.P. Soares, T. Satoh, S. Akira, T. Hai, C. de Guzman Strong, K. Auclair, T.P. Roddy, S.A. Biller, M. Jovanovic, E. Klechevsky, K.M. Stewart, G. J. Randolph, M.N. Artyomov, Electrophilic properties of itaconate and derivatives

regulate the IkappaBzeta-ATF3 inflammatory axis, Nature 556 (7702) (2018) 501–504.
[15] L.A.J. O'Neill, M.N. Artyomov, Itaconate: the poster child of metabolic reprogramming in macrophage function, Nat. Rev. Immunol. 19 (5) (2019) 273–281.
[16] Z. Zhang, C. Chen, F. Yang, Y.X. Zeng, P. Sun, P. Liu, X. Li, Itaconate is a lysosomal inducer that promotes antibacterial innate immunity, Mol. Cell 82 (15) (2022) 2844–2857 e10.
[17] E.L. Mills, D.G. Ryan, H.A. Prag, D. Dikovskaya, D. Menon, Z. Zaslona, M. P. Jedrychowski, A.S.H. Costa, M. Higgins, E. Hams, J. Szpyt, M.C. Runtsch, M. S. King, J.F. McGouran, R. Fischer, B.M. Kessler, A.F. McGettrick, M.M. Hughes, R.G. Carroll, L.M. Booty, E.V. Knatko, P.J. Meakin, M.L.J. Ashford, L.K. Modis, G. Brunori, D.C. Sevin, P.G. Fallon, S.T. Caldwell, E.R.S. Kunji, E.T. Chouchani, C. Frezza, A.T. Dinkova-Kostova, R.C. Hartley, M.P. Murphy, L.A. O'Neill, Itaconate is an anti-inflammatory metabolite that activates Nrf2 via alkylation of KEAP1, Nature 556 (7699) (2018) 113–117.
[18] A. Hooftman, S. Angiari, S. Hester, S.E. Corcoran, M.C. Runtsch, C. Ling, M. C. Ruzek, P.F. Slivka, A.F. McGettrick, K. Banahan, M.M. Hughes, A.D. Irvine, R. Fischer, L.A.J. O'Neill, The immunomodulatory metabolite itaconate modifies NLRP3 and inhibits inflammasome activation, Cell Metabol. 32 (3) (2020) 468–478 e7.
[19] M.C. Runtsch, S. Angiari, A. Hooftman, R. Wadhwa, Y. Zhang, Y. Zheng, J. S. Spina, M.C. Ruzek, M.A. Argiriadi, A.F. McGettrick, R.S. Mendez, A. Zotta, C. G. Peace, A. Walsh, R. Chirillo, E. Hams, P.G. Fallon, R. Jayamaran, K. Dua, A. C. Brown, R.Y. Kim, J.C. Horvat, P.M. Hansbro, C. Wang, L.A.J. O'Neill, Itaconate and itaconate derivatives target JAK1 to suppress alternative activation of macrophages, Cell Metabol. 34 (3) (2022) 487–501 e8.
[20] W. Qin, Y. Zhang, H. Tang, D. Liu, Y. Chen, Y. Liu, C. Wang, Chemoproteomic profiling of itaconation by bioorthogonal probes in inflammatory macrophages, J. Am. Chem. Soc. 142 (25) (2020) 10894–10898.
[21] Y. Zhang, W. Qin, D. Liu, Y. Liu, C. Wang, Chemoproteomic profiling of itaconations in *Salmonella*, Chem. Sci. 12 (17) (2021) 6059–6063.
[22] S.A. Riquelme, K. Liimatta, T. Wong Fok Lung, B. Fields, D. Ahn, D. Chen, C. Lozano, Y. Saenz, A.C. Uhlemann, B.C. Kahl, C.J. Britto, E. DiMango, A. Prince, *Pseudomonas aeruginosa* utilizes host-derived itaconate to redirect its metabolism to promote biofilm formation, Cell Metabol. 31 (6) (2020) 1091–1106 e6.
[23] E. Braude, F. Nachod, Determination of the Organic Structures by Physical Methods, Academic Press, New Yorck, 1955.
[24] D. Duncan, A. Lupien, M.A. Behr, K. Auclair, Effect of pH on the antimicrobial activity of the macrophage metabolite itaconate, Microbiology (Read.) 167 (5) (2021).
[25] P. Chandrangsu, V.V. Loi, H. Antelmann, J.D. Helmann, The role of bacillithiol in Gram-positive firmicutes, Antioxidants Redox Signal. 28 (6) (2018) 445–462.
[26] H. Antelmann, Chapter 12: Redox signalling mechanisms during host-pathogen interactions in the human pathogen *Staphylococcus aureus*, in: Y.-W. Tang, M. Hindiyeh, D. Liu, A. Sails, P. Spearman, Z. Zhan (Eds.), Molecular Medical Microbiology, Academic Press, 2023.
[27] N. Linzner, V.V. Loi, V.N. Fritsch, H. Antelmann, Thiol-based redox switches in the major pathogen *Staphylococcus aureus*, Biol. Chem. 402 (3) (2021) 333–361.
[28] M. Hillion, H. Antelmann, Thiol-based redox switches in prokaryotes, Biol. Chem. 396 (5) (2015) 415–444.
[29] P.R. Chen, P. Brugarolas, C. He, Redox signaling in human pathogens, Antioxidants Redox Signal. 14 (6) (2011) 1107–1118.
[30] M.J. Horsburgh, M.O. Clements, H. Crossley, E. Ingham, S.J. Foster, PerR controls oxidative stress resistance and iron storage proteins and is required for virulence in *Staphylococcus aureus*, Infect. Immun. 69 (6) (2001) 3744–3754.
[31] C.J. Ji, J.H. Kim, Y.B. Won, Y.E. Lee, T.W. Choi, S.Y. Ju, H. Youn, J.D. Helmann, J.W. Lee, *Staphylococcus aureus* PerR Is a hypersensitive hydrogen peroxide sensor using iron-mediated histidine oxidation, J. Biol. Chem. 290 (33) (2015) 20374–20386.
[32] B.K. Chi, K. Gronau, U. Mäder, B. Hessling, D. Becher, H. Antelmann, *S*-bacillithiolation protects against hypochlorite stress in *Bacillus subtilis* as revealed by transcriptomics and redox proteomics, Mol. Cell. Proteomics 10 (11) (2011). M111 009506.
[33] B.K. Chi, A.A. Roberts, T.T. Huyen, K. Bäsell, D. Becher, D. Albrecht, C. J. Hamilton, H. Antelmann, *S*-bacillithiolation protects conserved and essential proteins against hypochlorite stress in firmicutes bacteria, Antioxidants Redox Signal. 18 (11) (2013) 1273–1295.
[34] M. Imber, N.T.T. Huyen, A.J. Pietrzyk-Brzezinska, V.V. Loi, M. Hillion, J. Bernhardt, L. Thärichen, K. Kolsek, M. Saleh, C.J. Hamilton, L. Adrian, F. Gräter, M.C. Wahl, H. Antelmann, Protein S-bacillithiolation functions in thiol protection and redox regulation of the glyceraldehyde-3-phosphate dehydrogenase Gap in *Staphylococcus aureus* under hypochlorite stress, Antioxidants Redox Signal. 28 (6) (2018) 410–430.
[35] M. Imber, A.J. Pietrzyk-Brzezinska, H. Antelmann, Redox regulation by reversible protein *S*-thiolation in Gram-positive bacteria, Redox Biol. 20 (2019) 130–145.
[36] V.V. Loi, T. Busche, K. Tedin, J. Bernhardt, J. Wollenhaupt, N.T.T. Huyen, C. Weise, J. Kalinowski, M.C. Wahl, M. Fulde, H. Antelmann, Redox-sensing under hypochlorite stress and infection conditions by the Rrf2-family repressor HypR in *Staphylococcus aureus*, Antioxidants Redox Signal. 29 (7) (2018) 615–636.
[37] H.L. Shearer, V.V. Loi, P. Weiland, G. Bange, F. Altegoer, M.B. Hampton, H. Antelmann, N. Dickerhof, MerA functions as a hypothiocyanous acid reductase and defense mechanism in *Staphylococcus aureus*, Mol. Microbiol. 119 (4) (2023) 456–470.
[38] X. Zhu, H. Lei, J. Wu, J.V. Li, H. Tang, Y. Wang, Systemic responses of BALB/c mice to *Salmonella typhimurium* infection, J. Proteome Res. 13 (10) (2014) 4436–4445.
[39] S.J. Hersch, W.W. Navarre, The *Salmonella* LysR family regulator RipR activates the SPI-13-Encoded itaconate degradation cluster, Infect. Immun. 88 (10) (2020).
[40] K. Dörries, M. Lalk, Metabolic footprint analysis uncovers strain specific overflow metabolism and D-isoleucine production of *Staphylococcus aureus* COL and HG001, PLoS One 8 (12) (2013), e81500.
[41] V.V. Loi, M. Harms, M. Müller, N.T.T. Huyen, C.J. Hamilton, F. Hochgräfe, J. Pane-Farre, H. Antelmann, Real-time imaging of the bacillithiol redox potential in the human pathogen *Staphylococcus aureus* using a genetically encoded bacilliredoxin-fused redox biosensor, Antioxidants Redox Signal. 26 (15) (2017) 835–848.
[42] B.K. Chi, T. Busche, K. Van Laer, K. Bäsell, D. Becher, L. Clermont, G.M. Seibold, M. Persicke, J. Kalinowski, J. Messens, H. Antelmann, Protein S-mycothiolation functions as redox-switch and thiol protection mechanism in *Corynebacterium glutamicum* under hypochlorite stress, Antioxidants Redox Signal. 20 (4) (2014) 589–605.
[43] B. Langmead, S.L. Salzberg, Fast gapped-read alignment with Bowtie 2, Nat. Methods 9 (4) (2012) 357–359.
[44] H. Li, B. Handsaker, A. Wysoker, T. Fennell, J. Ruan, N. Homer, G. Marth, G. Abecasis, R. Durbin, S, Genome project data processing, the sequence alignment/map format and SAMtools, Bioinformatics 25 (16) (2009) 2078–2079.
[45] R. Hilker, K.B. Stadermann, O. Schwengers, E. Anisiforov, S. Jaenicke, B. Weisshaar, T. Zimmermann, A. Goesmann, ReadXplorer 2-detailed read mapping analysis and visualization from one single source, Bioinformatics 32 (24) (2016) 3702–3708.
[46] M.I. Love, W. Huber, S. Anders, Moderated estimation of fold change and dispersion for RNA-seq data with DESeq2, Genome Biol. 15 (12) (2014) 550.
[47] M. Wetzstein, U. Völker, J. Dedio, S. Lobau, U. Zuber, M. Schiesswohl, C. Herget, M. Hecker, W. Schumann, Cloning, sequencing, and molecular analysis of the *dnaK* locus from *Bacillus subtilis*, J. Bacteriol. 174 (10) (1992) 3300–3310.
[48] T. Tam le, C. Eymann, D. Albrecht, R. Sietmann, F. Schauer, M. Hecker, H. Antelmann, Differential gene expression in response to phenol and catechol reveals different metabolic activities for the degradation of aromatic compounds in *Bacillus subtilis*, Environ. Microbiol. 8 (8) (2006) 1408–1427.
[49] N. Linzner, V.V. Loi, H. Antelmann, The catalase KatA contributes to microaerophilic H_2O_2 priming to acquire an improved oxidative stress resistance in *Staphylococcus aureus*, Antioxidants 11 (9) (2022).
[50] V.N. Fritsch, V.V. Loi, B. Kuropka, M.C.H. Gruhlke, C. Weise, H. Antelmann, The MarR/DUF24-family QsrR repressor senses quinones and oxidants by thiol switch mechanisms in *Staphylococcus aureus*, Antioxid. Redox Signal.38 13-15 (2023) 877–895.
[51] C. UniProt, UniProt: the universal protein knowledgebase in 2023, Nucleic Acids Res. 51 (D1) (2023) D523–D531.
[52] Y. Perez-Riverol, J. Bai, C. Bandla, D. Garcia-Seisdedos, S. Hewapathirana, S. Kamatchinathan, D.J. Kundu, A. Prakash, A. Frericks-Zipper, M. Eisenacher, M. Walzer, S. Wang, A. Brazma, J.A. Vizcaino, The PRIDE database resources in 2022: a hub for mass spectrometry-based proteomics evidences, Nucleic Acids Res. 50 (D1) (2022) D543–D552.
[53] K. Dörries, R. Schlueter, M. Lalk, Impact of antibiotics with various target sites on the metabolome of *Staphylococcus aureus*, Antimicrob. Agents Chemother. 58 (12) (2014) 7151–7163.
[54] A. Troitzsch, V.V. Loi, K. Methling, D. Zühlke, M. Lalk, K. Riedel, J. Bernhardt, E. M. Elsayed, G. Bange, H. Antelmann, J. Pane-Farre, Carbon source-dependent reprogramming of anaerobic metabolism in *Staphylococcus aureus*, J. Bacteriol. 203 (8) (2021) e00639–20.
[55] A. Rath, S. Rautenschlein, J. Rzeznitzeck, M. Lalk, K. Methling, I. Rychlik, E. Peh, S. Kittler, K.H. Waldmann, A. von Altrock, Investigation on the colonisation of *Campylobacter* strains in the pig intestine depending on available metabolites, Comp. Immunol. Microbiol. Infect. Dis. 88 (2022), 101865.
[56] C. Zhou, P.D. Fey, The acid response network of *Staphylococcus aureus*, Curr. Opin. Microbiol. 55 (2020) 67–73.
[57] U. Mäder, P. Nicolas, M. Depke, J. Pane-Farre, M. Debarbouille, M.M. van der Kooi-Pol, C. Guerin, S. Derozier, A. Hiron, H. Jarmer, A. Leduc, S. Michalik, E. Reilman, M. Schaffer, F. Schmidt, P. Bessieres, P. Noirot, M. Hecker, T. Msadek, U. Völker, J.M. van Dijl, *Staphylococcus aureus* transcriptome architecture: from laboratory to infection-mimicking conditions, PLoS Genet. 12 (4) (2016), e1005962.
[58] A. Price-Whelan, C.K. Poon, M.A. Benson, T.T. Eidem, C.M. Roux, J.M. Boyd, P. M. Dunman, V.J. Torres, T.A. Krulwich, Transcriptional profiling of *Staphylococcus aureus* during growth in 2 M NaCl leads to clarification of physiological roles for Kdp and Ktr K+ uptake systems, mBio 4 (4) (2013) e00407–13.
[59] B. Weinrick, P.M. Dunman, F. McAleese, E. Murphy, S.J. Projan, Y. Fang, R. P. Novick, Effect of mild acid on gene expression in *Staphylococcus aureus*, J. Bacteriol. 186 (24) (2004) 8407–8423.
[60] K. Gunka, F.M. Commichau, Control of glutamate homeostasis in *Bacillus subtilis*: a complex interplay between ammonium assimilation, glutamate biosynthesis and degradation, Mol. Microbiol. 85 (2) (2012) 213–224.
[61] C. Zhou, F. Bhinderwala, M.K. Lehman, V.C. Thomas, S.S. Chaudhari, K. J. Yamada, K.W. Foster, R. Powers, T. Kielian, P.D. Fey, Urease is an essential component of the acid response network of *Staphylococcus aureus* and is required for a persistent murine kidney infection, PLoS Pathog. 15 (1) (2019), e1007538.

[62] S.J. Yang, K.C. Rice, R.J. Brown, T.G. Patton, L.E. Liou, Y.H. Park, K.W. Bayles, A LysR-type regulator, CidR, is required for induction of the *Staphylococcus aureus cidABC* operon, J. Bacteriol. 187 (17) (2005) 5893–5900.

[63] S.J. Yang, P.M. Dunman, S.J. Projan, K.W. Bayles, Characterization of the *Staphylococcus aureus* CidR regulon: elucidation of a novel role for acetoin metabolism in cell death and lysis, Mol. Microbiol. 60 (2) (2006) 458–468.

[64] V.N. Fritsch, V.V. Loi, T. Busche, A. Sommer, K. Tedin, D.J. Nürnberg, J. Kalinowski, J. Bernhardt, M. Fulde, H. Antelmann, The MarR-type repressor MhqR confers quinone and antimicrobial resistance in *Staphylococcus aureus*, Antioxidants Redox Signal. 31 (16) (2019) 1235–1252.

[65] R.S. Flannagan, R.C. Kuiack, M.J. McGavin, D.E. Heinrichs, *Staphylococcus aureus* uses the GraXRS regulatory system to sense and adapt to the acidified phagolysosome in macrophages, mBio 9 (4) (2018) e01143–18.

[66] S. Schlag, S. Fuchs, C. Nerz, R. Gaupp, S. Engelmann, M. Liebeke, M. Lalk, M. Hecker, F. Gotz, Characterization of the oxygen-responsive NreABC regulon of *Staphylococcus aureus*, J. Bacteriol. 190 (23) (2008) 7847–7858.

[67] M. Liebeke, K. Dörries, D. Zühlke, J. Bernhardt, S. Fuchs, J. Pane-Farre, S. Engelmann, U. Völker, R. Bode, T. Dandekar, U. Lindequist, M. Hecker, M. Lalk, A metabolomics and proteomics study of the adaptation of *Staphylococcus aureus* to glucose starvation, Mol. Biosyst. 7 (4) (2011) 1241–1253.

[68] C.R. Halsey, S. Lei, J.K. Wax, M.K. Lehman, A.S. Nuxoll, L. Steinke, M. Sadykov, R. Powers, P.D. Fey, Amino acid catabolism in *Staphylococcus aureus* and the function of carbon catabolite repression, mBio 8 (1) (2017) e01434–16.

[69] D.F. Niven, R.E. Jeacocke, W.A. Hamilton, The membrane potential as the driving force for the accumulation of lysine by *Staphylococcus aureus*, FEBS Lett. 29 (3) (1973) 248–252.

[70] M.S. Zeden, I. Kviatkovski, C.F. Schuster, V.C. Thomas, P.D. Fey, A. Grundling, Identification of the main glutamine and glutamate transporters in *Staphylococcus aureus* and their impact on c-di-AMP production, Mol. Microbiol. 113 (6) (2020) 1085–1100.

[71] L.I. Leichert, F. Gehrke, H.V. Gudiseva, T. Blackwell, M. Ilbert, A.K. Walker, J. R. Strahler, P.C. Andrews, U. Jakob, Quantifying changes in the thiol redox proteome upon oxidative stress in vivo, Proc. Natl. Acad. Sci. U. S. A. 105 (24) (2008) 8197–8202.

[72] K.L. Tomlinson, A.S. Prince, T. Wong Fok Lung, Immunometabolites drive bacterial adaptation to the airway, Front. Immunol. 12 (2021), 790574.

[73] M. Chen, H. Sun, M. Boot, L. Shao, S.J. Chang, W. Wang, T.T. Lam, M. Lara-Tejero, E.H. Rego, J.E. Galan, Itaconate is an effector of a Rab GTPase cell-autonomous host defense pathway against *Salmonella*, Science 369 (6502) (2020) 450–455.

[74] M.J. Geisow, P. D'Arcy Hart, M.R. Young, Temporal changes of lysosome and phagosome pH during phagolysosome formation in macrophages: studies by fluorescence spectroscopy, J. Cell Biol. 89 (3) (1981) 645–652.

[75] M.B. Hampton, N. Dickerhof, Inside the phagosome: a bacterial perspective, Immunol. Rev. 314 (1) (2023) 197–209.

[76] I.N. Hirshfield, S. Terzulli, C. O'Byrne, Weak organic acids: a panoply of effects on bacteria, Sci. Prog. 86 (Pt 4) (2003) 245–269.

[77] T.M. Rode, T. Moretro, S. Langsrud, O. Langsrud, G. Vogt, A. Holck, Responses of *Staphylococcus aureus* exposed to HCl and organic acid stress, Can. J. Microbiol. 56 (9) (2010) 777–792.

[78] E. Bore, S. Langsrud, O. Langsrud, T.M. Rode, A. Holck, Acid-shock responses in *Staphylococcus aureus* investigated by global gene expression analysis, Microbiology (Read.) 153 (Pt 7) (2007) 2289–2303.

[79] E.R. Kashket, S.L. Barker, Effects of potassium ions on the electrical and pH gradients across the membrane of *Streptococcus lactis* cells, J. Bacteriol. 130 (3) (1977) 1017–1023.

[80] R.G. Kroll, I.R. Booth, The role of potassium transport in the generation of a pH gradient in *Escherichia coli*, Biochem. J. 198 (3) (1981) 691–698.

[81] R.G. Kroll, I.R. Booth, The relationship between intracellular pH, the pH gradient and potassium transport in *Escherichia coli*, Biochem. J. 216 (3) (1983) 709–716.

[82] E.P. Bakker, W.E. Mangerich, Interconversion of components of the bacterial proton motive force by electrogenic potassium transport, J. Bacteriol. 147 (3) (1981) 820–826.

[83] S.G. Dashper, E.C. Reynolds, pH regulation by *Streptococcus mutans*, J. Dent. Res. 71 (5) (1992) 1159–1165.

[84] M. Follmann, M. Becker, I. Ochrombel, V. Ott, R. Krämer, K. Marin, Potassium transport in *Corynebacterium glutamicum* is facilitated by the putative channel protein CglK, which is essential for pH homeostasis and growth at acidic pH, J. Bacteriol. 191 (9) (2009) 2944–2952.

[85] W. Epstein, The roles and regulation of potassium in bacteria, Prog. Nucleic Acid Res. Mol. Biol. 75 (2003) 293–320.

[86] C.M. Gries, M.R. Sadykov, L.L. Bulock, S.S. Chaudhari, V.C. Thomas, J.L. Bose, K. W. Bayles, Potassium uptake modulates *Staphylococcus aureus* metabolism, mSphere 1 (3) (2016).

[87] A. Gründling, Potassium uptake systems in *Staphylococcus aureus*: new stories about ancient systems, mBio 4 (5) (2013), e00784-13.

[88] F. Lamret, J. Varin-Simon, F. Velard, C. Terryn, C. Mongaret, M. Colin, S. C. Gangloff, F. Reffuveille, *Staphylococcus aureus* strain-dependent biofilm formation in bone-like environment, Front. Microbiol. 12 (2021), 714994.

[89] T. Busche, M. Hillion, V. Van Loi, D. Berg, B. Walther, T. Semmler, B. Strommenger, W. Witte, C. Cuny, A. Mellmann, M.A. Holmes, J. Kalinowski, L. Adrian, J. Bernhardt, H. Antelmann, Comparative secretome analyses of human and zoonotic *Staphylococcus aureus* isolates CC8, CC22, and CC398, Mol. Cell. Proteomics 17 (12) (2018) 2412–2433.

[90] M.M. Alreshidi, R.H. Dunstan, M.M. Macdonald, J. Gottfries, T.K. Roberts, The uptake and release of amino acids by *Staphylococcus aureus* at mid-exponential and stationary phases and their corresponding responses to changes in temperature, pH and osmolality, Front. Microbiol. 10 (2019) 3059.

[91] M.S. Zeden, O. Burke, M. Vallely, C. Fingleton, J.P. O'Gara, Exploring amino acid and peptide transporters as therapeutic targets to attenuate virulence and antibiotic resistance in *Staphylococcus aureus*, PLoS Pathog. 17 (1) (2021), e1009093.

[92] E. Bremer, R. Krämer, Responses of microorganisms to osmotic stress, Annu. Rev. Microbiol. 73 (2019) 313–334.

[93] J. Stülke, L. Krüger, Cyclic di-AMP signaling in bacteria, Annu. Rev. Microbiol. 74 (2020) 159–179.

[94] C.F. Schuster, L.E. Bellows, T. Tosi, I. Campeotto, R.M. Corrigan, P. Freemont, A. Gründling, The second messenger c-di-AMP inhibits the osmolyte uptake system OpuC in *Staphylococcus aureus*, Sci. Signal. 9 (441) (2016) ra81.

[95] J.A. Moscoso, H. Schramke, Y. Zhang, T. Tosi, A. Dehbi, K. Jung, A. Gründling, Binding of cyclic di-AMP to the *Staphylococcus aureus* sensor kinase KdpD occurs via the universal stress protein domain and downregulates the expression of the Kdp potassium transporter, J. Bacteriol. 198 (1) (2016) 98–110.

[96] C. Detsch, J. Stülke, Ammonium utilization in *Bacillus subtilis:* transport and regulatory functions of NrgA and NrgB, Microbiology (Read.) 149 (Pt 11) (2003) 3289–3297.

[97] C.T. Huang, M.L. Chen, L.L. Huang, I.F. Mao, Uric acid and urea in human sweat, Chin. J. Physiol. 45 (3) (2002) 109–115.

[98] I.D. Weiner, W.E. Mitch, J.M. Sands, Urea and ammonia metabolism and the control of renal nitrogen excretion, Clin. J. Am. Soc. Nephrol. 10 (8) (2015) 1444–1458.

[99] B. Foxman, The epidemiology of urinary tract infection, Nat. Rev. Urol. 7 (12) (2010) 653–660.

[100] T.J. Lasisi, Y.R. Raji, B.L. Salako, Salivary creatinine and urea analysis in patients with chronic kidney disease: a case control study, BMC Nephrol. 17 (2016) 10.

[101] K. Xu, Y. Wang, Y. Jian, T. Chen, Q. Liu, H. Wang, M. Li, L. He, *Staphylococcus aureus* ST1 promotes persistent urinary tract infection by highly expressing the urease, Front. Microbiol. 14 (2023), 1101754.

[102] M.O. Clements, S.P. Watson, S.J. Foster, Characterization of the major superoxide dismutase of *Staphylococcus aureus* and its role in starvation survival, stress resistance, and pathogenicity, J. Bacteriol. 181 (13) (1999) 3898–3903.

[103] K. Cosgrove, G. Coutts, I.M. Jonsson, A. Tarkowski, J.F. Kokai-Kun, J.J. Mond, S. J. Foster, Catalase (KatA) and alkyl hydroperoxide reductase (AhpC) have compensatory roles in peroxide stress resistance and are required for survival, persistence, and nasal colonization in *Staphylococcus aureus*, J. Bacteriol. 189 (3) (2007) 1025–1035.

[104] K.S. Makarova, V.A. Ponomarev, E.V. Koonin, Two C or not two C: recurrent disruption of Zn-ribbons, gene duplication, lineage-specific gene loss, and horizontal gene transfer in evolution of bacterial ribosomal proteins, Genome Biol. 2 (9) (2001). RESEARCH 0033.

[105] S.E. Gabriel, J.D. Helmann, Contributions of Zur-controlled ribosomal proteins to growth under zinc starvation conditions, J. Bacteriol. 191 (19) (2009) 6116–6122.